

# Observationally guided models for the solar dynamo and the role of the surface field

Robert H. Cameron and Manfred Schüssler

Max Planck Institute for Solar System Research,  
Justus-von-Liebig-Weg 3, 37077 Göttingen, Germany.

## Abstract

Theoretical models for the solar dynamo range from simple low-dimensional “toy models” to complex 3D-MHD simulations. Here we mainly discuss approaches that are motivated and guided by solar (and stellar) observations. We give a brief overview of the evolution of solar dynamo models since 1950s, focussing upon the development of the Babcock-Leighton approach between its introduction in the 1960s and its revival in the 1990s after being long overshadowed by mean-field turbulent dynamo theory. We summarize observations and simple theoretical deliberations that demonstrate the crucial role of the surface fields in the dynamo process and give quantitative analyses of the generation and loss of toroidal flux in the convection zone as well as of the production of poloidal field resulting from flux emergence at the surface. Furthermore, we discuss possible nonlinearities in the dynamo process suggested by observational results and present models for the long-term variability of solar activity motivated by observations of magnetically active stars and the inherent randomness of the dynamo process.

**Keywords:** solar activity, solar cycle, dynamo

## 1 Introduction

Studies of solar and stellar dynamos face a problem of utter complexity, i.e., the interaction of turbulent convection with rotation and magnetic field in a highly stratified medium, covering wide ranges of spatial and temporal scales. Attempts to directly attack this problem with numerical 3D-MHD simulations have made significant progress in recent years (e.g., [Charbonneau, 2020](#);

Browning and et al, 2023), but are still severely limited in spatial resolution, so that a faithful representation of the solar cycle has not been achieved so far. All other approaches to the dynamo problem resort to simplifications in order to obtain a tractable task. They largely rely on the surprising amount of regularity shown by the solar cycle, e.g., Hale’s polarity rules and the systematic tilt of sunspot groups (Joy’s law), the butterfly diagram, and the regular reversals of the global dipole field (Hathaway, 2015). These regularities suggest simplified concepts, such as the generation of azimuthal (toroidal) magnetic flux through winding of meridional (poloidal) magnetic field lines by differential rotation (Cowling, 1953) or the formation of bipolar sunspot groups by the emergence of buoyantly rising magnetic flux tubes (Parker, 1955b).

A variety of models addressing various aspects of the dynamo problem has been developed. These range from rather ad-hoc “toy models” over sophisticated two-scale approaches, pioneered by the model of Parker (1955a) and by mean-field theory of turbulent MHD flows (see review by Brandenburg et al, 2023) to 2D/3D flux-transport dynamo models including various physical processes considered to be relevant for the dynamo (see reviews by Charbonneau, 2020; Hazra et al, 2023).

The simplest “model” in the literature is probably due to Barnes et al (1980). These authors considered a digital narrow-band filtering of Gaussian white noise, corresponding to a randomly disturbed periodic signal that could be illustrated by a “pendulum pelted with peas” (Yule, 1927). The results of their short computer program (15 lines!) exhibit a very similar kind of variability as shown by the sunspot record, including the occurrence of extended periods of low activity (grand minima). The important lesson from this result for models of the solar dynamo is that even a striking similarity of their output with records of solar activity alone does not necessarily imply the validity of a model.

In this paper, we focus upon models of the solar dynamo as well as for the cyclic generation and removal of magnetic flux that are guided by solar (and also stellar) observations. The motivation for such approaches comes from the fact that the very complex interactions in the convection zone can lead to comparably simple results, such as the stable differential rotation in latitude, the meridional circulation, the polarity rules of sunspot groups, or the butterfly diagram of magnetic flux emergence. This might perhaps be compared to the flow of water in a watermill: although the detailed turbulent flow pattern is utterly complex, the general result is simple: water flows down the potential well and faithfully drives the wheel. The paradigm of observationally motivated models is the scenario of Babcock (1961), which was later extended and put in a mathematical form by Leighton (1969). These seminal papers paved the way for what are now generally called Babcock-Leighton-type models of the solar dynamo.

The plan of this paper is as follows. In Sec. 2 we describe the principles of the Babcock-Leighton scenario and review the evolution of dynamo models until the end of the 1980s, when mounting empirical evidence led to the renaissance

of Babcock-Leighton dynamo models after an extended period of near oblivion. The generation and removal of toroidal and poloidal magnetic flux in the Sun and the crucial role of the observable surface field are discussed in Sec. 3. Nonlinearity of the dynamo process, predictability, and models for the long-term variability of solar activity are considered in Sec. 4. Sec. 5 gives a brief outlook.

## 2 The Babcock-Leighton approach and the evolution of models for the solar dynamo

The seminal paper of Babcock (1961) lays out a purely observationally based scenario for the 11/22-year solar cycle. In a first step, the poloidal magnetic flux connected to the global dipole field is wound up by latitudinal differential rotation in the convection zone. This generates oppositely directed subsurface belts of toroidal field in both hemispheres. Subsequent instability, buoyant rise, and emergence of toroidal flux at the surface produces bipolar magnetic regions (BMRs) and sunspot groups in accordance with Hale's polarity rules. These regions are observed to be systematically tilted in the sense that the magnetic polarity leading in the direction of rotation is nearer to the equator than the following polarity. This tilt, together with the dispersal of the BMRs in the course of time, leads to preferred transport of leading-polarity flux over the equator, so that a surplus of the respective following-polarity flux builds up in both hemispheres. Poleward transport of this flux by convection and meridional circulation leads to the reversal of the polar fields and the buildup of an oppositely directed dipole field, a process already suggested by Babcock and Babcock (1955). This entails the generation and emergence of a reversed toroidal field followed by another reversal of the dipole field, thus giving rise to the 22-year magnetic cycle.

Babcock (1961) already noted that the systematic tilt of the sunspot groups could be "... the result of Coriolis forces, which induce a vorticity in the whole of the fluid associated with a BMR when it rises to the surface." The Coriolis effect is also invoked in the concept of "cyclonic convection" of Parker (1955a) and in the mean-field scheme based on turbulence theory pioneered by Steenbeck and Krause (1966) and Steenbeck et al (1966). Possibly since both these approaches focus on the collective effect of a small-scale process (in the sense of a two-scale approach), neither Parker nor Steenbeck and coworkers apparently realized that the systematic tilt provides direct observational support for the action of the Coriolis effect as well a quantitative measure.

Leighton (1964) added a key component to Babcock's scenario in the form of a random-walk model for the quasi-diffusive transport of magnetic flux on the solar surface by supergranular convection. Subsequently, he put the Babcock model in the mathematical form of a one-dimensional dynamo equation (Leighton, 1969). It is not obvious why this Babcock-Leighton (BL) model fell into near oblivion for about two decades thereafter. In order to provide some

understanding for this development, a brief sketch of the evolution of solar dynamo studies from the early 1970s onward is given in what follows.

Perhaps since the mathematically involved mean-field theory was considered to provide a strong theoretical footing, models for the solar dynamo until the 1990s mostly relied on a mean-field turbulent “ $\alpha$ -effect” based on correlations between small-scale fields operating within the convection zone. To explain the equatorward-directed migration of the activity belts shown by the butterfly diagram, these models generally required an inwardly increasing rotation rate,  $d\Omega/dr < 0$  (Köhler, 1973; Yoshimura, 1975). The effect of the observed strong latitudinal differential rotation was thought to be of secondary importance. Consequently, both key processes for the turbulent dynamo, radial differential rotation and  $\alpha$ -effect, were assumed to operate in the solar interior, thus inaccessible to observation at that time. Therefore, the corresponding model parameters were largely unconstrained. The observable evolution of the surface field was seen as a mere epiphenomenon of a dynamo process operating deeply hidden in the convection zone and served solely as an observational constraint for the models.

The foundations of this approach were undermined when helioseismology made it possible to measure the differential rotation in the convection zone. It turned out that (except for a shallow near-surface shear layer) the increase of the rotation rate with depth required by these models is absent in the bulk of the convection zone (see review by Howe, 2009). On the other hand, the rotation rate at the bottom of the convection zone showed a steep radial gradient across the “tachocline” (Brown et al, 1989), such that  $d\Omega/dr < 0$  in solar latitudes  $\geq 45$  deg and  $d\Omega/dr > 0$  in lower latitudes. Some years before, Galloway and Weiss (1981) already had suggested that the solar dynamo should work in a stably stratified layer of overshooting convection below the bottom of the convection zone in order to avoid the rapid buoyant loss of toroidal magnetic flux inferred by Parker (1975). These results led to the concept of turbulent dynamo action within the overshoot layer/tachocline (e.g., Rüdiger and Brandenburg, 1995) or near its interface with the convection zone proper (Parker, 1993), where a properly chosen combination of the signs of  $\alpha$ -effect and radial gradient of the rotation rate could provide the correct conditions for equatorward propagating dynamo waves and activity belts (e.g., Tobias, 1996; Charbonneau and MacGregor, 1997). This approach was complemented by studies of equilibrium, stability, and dynamics of thin magnetic flux tubes starting with Spruit and van Ballegoijen (1982), Choudhuri and Gilman (1987), and Moreno-Insertis et al (1992). Such studies (see reviews by Fan, 2021; Isik and etal, 2023) indicated that the toroidal field in the overshoot region must be amplified to about  $10^5$  G before becoming unstable (Ferriz-Mas and Schüssler, 1993, 1995) and rising to the surface to form bipolar magnetic regions within the latitude range shown by the butterfly diagram (Schüssler et al, 1994). Twisting of the rising flux tubes due to the Coriolis force then leads to tilt angles consistent with observation (Fan et al, 1994; Caligari et al, 1995).

Although the combination of tachocline/overshoot layer dynamos and the dynamics of thin flux tubes offered a comprehensive picture from the generation of magnetic flux up to its emergence at the surface, these models relied on a number of untested assumptions and simplifications, so that their predictive power remained rather limited. In the course of time, a number of theoretical considerations and observational results cast severe doubt upon the validity of this approach:

- The total energy of a toroidal field of  $10^5$  Gauss at the bottom of the convection zone would be comparable to the energy in the differential rotation of the tachocline (Rempel, 2006). However, a corresponding strong variation of the differential rotation in the lower convection zone and tachocline in the course of the 11-year activity cycle is not observed (Basu and Antia, 2019). Moreover, the interface between radiative core and convection zone cannot support much shear stress (Spruit, 2011). Consequently, the radial differential rotation in the tachocline (mainly reflecting the transition from latitudinally differential rotation in the convection zone to nearly rigid rotation below) cannot generate a sizeable amount of toroidal magnetic flux unless being maintained by a very powerful downward transport of angular momentum.
- The latitudinal differential rotation is sufficient to create the total toroidal flux covered by the emergence of bipolar magnetic regions and sunspot groups. At the same time, the contribution of the observed radial differential rotation in the convection zone is only a few percent of that of the latitudinal differential rotation (Cameron and Schüssler, 2015). Moreover, the radial shear in the tachocline is strong in high latitudes and weak in low latitudes, thus unfavorable for toroidal flux generation in low latitudes.
- Helioseismology indicates that the overshoot layer is much more strongly subadiabatic than assumed in the models for the storage and stability of toroidal flux (Christensen-Dalsgaard et al, 2011). On the other hand, part of the lower convection zone could be subadiabatically stratified (e.g., Spruit, 1997; Hotta, 2017).
- Observations of magnetically active stars show that partly and fully convective stars follow the same activity-rotation law (Wright and Drake, 2016; Reiners et al, 2022), thus questioning the relevance of convective overshoot and the existence of a tachocline for the dynamo process. Furthermore, even very cool, fully convective dwarfs (beyond spectral type M7) can exhibit activity cycles (Route, 2016).
- 3D-MHD simulations demonstrate the formation of super-equipartition magnetic flux concentrations and buoyantly rising flux loops within a simulated convection zone without overshoot and tachocline (Nelson et al, 2014; Fan and Fang, 2014; Chen et al, 2017).
- If emerged magnetic structures were “anchored” near to the bottom of the convection zone, they should show slower rotation than that of the surface

plasma below about  $\pm 30$  deg latitude according to the helioseismically determined rotation profile. However, magnetic structures are observed rotate faster than the plasma at the surface (e.g., [Howard, 1996](#)).

A new twist came when observations of a systematic poleward-directed meridional flow at the surface pioneered by [Duvall \(1979\)](#) and [Howard \(1979\)](#) became established during the 1980s (see review by [Hanasoge, 2022](#)). This led to the suggestion that the associated deep return flow within the convection zone could transport toroidal flux equatorward. Models of flux-transport dynamos (FTDs) that rely upon this concept can provide a butterfly diagram consistent with observations regardless of the sign of the radial gradient of the rotation rate ([Wang and Sheeley, 1991](#); [Durney, 1995](#); [Choudhuri et al, 1995](#)). A recent review of FTD models has been provided by [Hazra et al \(2023\)](#).

The confirmation of the systematic poleward surface flow also sparked the development of simulation models for the transport of magnetic flux at the solar surface on solar-cycle time scales, pioneered by the NRL group ([DeVore et al, 1984](#); [Wang et al, 1989b](#)). Such Surface Flux Transport (SFT) models (see reviews by [Mackay and Yeates, 2012](#); [Yeates et al, 2023](#)) assume passive transport of vertically (radially) orientated magnetic flux by surface flows. Comparison of SFT simulations with observed synoptic magnetograms shows that the evolution of the surface flux can be faithfully described by flux emergence in systematically tilted bipolar magnetic regions followed by passive flux transport by differential rotation, meridional flow, and supergranular flows (the latter mostly being treated as a diffusion-like random walk, cf. [Leighton, 1964](#)), and flux cancellation. In particular, the models confirm the buildup of polar fields due to the preferred transport of following-polarity flux toward the poles ([Wang et al, 1989a](#)).

The success of the SFT simulations led to the re-appraisal of the BL approach for the (re)generation of the poloidal field in the course of the dynamo process ([Giovannelli, 1985](#); [Wang and Sheeley, 1991](#)), typically in connection with equatorward flux transport by meridional flow in the convection zone as Flux Transport Dynamo (FTD) models ([Wang et al, 1991](#); [Charbonneau, 2020](#); [Hazra et al, 2023](#)). In the course of time, further lines of evidence for the validity of the BL approach and the crucial role of the surface flux for the solar dynamo became apparent:

- SFT models reproduce the evolution of the surface field, particularly the poleward drift of the following-polarity surface field leading to the buildup of the polar fields and the axial dipole (e.g., [Wang et al, 2002](#); [Baumann et al, 2004](#); [Jiang et al, 2014b](#); [Upton and Hathaway, 2014](#); [Whitbread et al, 2017](#)).
- The polar field strength around cycle minimum is strongly correlated with the amplitude of the subsequent activity maximum ([Legrand and Simon, 1981](#); [Wang and Sheeley, 2009](#); [Kitchatinov and Olemskoy, 2011b](#); [Hathaway and Upton, 2016](#)), thus providing the most faithful predictor of cycle strength ([Schatten et al, 1978](#); [Petrovay, 2020](#); [Kumar et al, 2021](#); [Bhowmik](#)

et al, 2023). In addition to confirming this correlation, Muñoz-Jaramillo et al (2013) showed that the “memory” of the system does not extend beyond one cycle.

- Cameron and Schüssler (2015) showed that the above correlation in fact reflects a causation: the net hemispheric toroidal flux generated during a half cycle results from the action of the latitudinal differential rotation on the poloidal flux connected to the polar fields (see Sec. 3.1 below).
- The observed azimuthal surface field (a proxy for flux emergence) evolves in accordance with an updated BL model (Cameron et al, 2018).

The timescale for the rise of flux loops formed by the toroidal field and the subsequent flux emergence is generally considered to be short compared to the cycle time scale. Therefore, BL dynamo models typically do not explicitly include these processes but rather incorporate a source term near the surface that is related to the deep-seated toroidal field in the convection zone (for a discussion of various approaches, see Choudhuri and Hazra, 2016). A few examples of two-dimensional axisymmetric dynamo models with different prescriptions for the BL source term are the studies of Durney (1997), Dikpati and Charbonneau (1999), Nandy and Choudhuri (2001), Chatterjee et al (2004), and Muñoz-Jaramillo et al (2010). More complete overviews have been provided by Charbonneau (2020) and Hazra et al (2023).

FTD/BL models mostly rely on radial differential rotation in the tachocline and often also assume penetration of the meridional flow into the stably stratified interior in order to “store” the toroidal magnetic flux at the bottom of the convection zone (e.g., Nandy and Choudhuri, 2002). In contrast, the 2D model of Zhang and Jiang (2022) exhibits no such penetration, but consistently includes the helioseismically determined differential rotation in the convection zone (including the near-surface shear layer), a one-cell meridional circulation, radial pumping keeping the surface field vertical and inhibiting diffusive loss of the toroidal field, and a BL source term. The generation of toroidal flux turns out to be strongly dominated by the latitudinal differential rotation in the bulk of the convection zone (see also Guerrero and de Gouveia Dal Pino, 2007; Muñoz-Jaramillo et al, 2009). The latitudinal propagation of the toroidal flux belts in the model of Zhang and Jiang (2022) is provided by a combination of flux transport by the equatorward meridional return flow and the latitude dependence of the latitudinal rotational shear generating toroidal magnetic flux, the latter as already envisaged by Babcock (1961). Test cases with removal of the radial shear in the tachocline or putting the numerical boundary above the tachocline does not significantly change the results of the model, thus strongly suggesting that the tachocline shear is indeed largely irrelevant for the dynamo (cf. Spruit, 2011; Brandenburg, 2005; Cameron and Schüssler, 2015).

Typically, FT/BL dynamo models are 2D (axisymmetric) or even 3D and time-dependent. Although they exhibit solar-like solutions for properly chosen values of the parameters (e.g., turbulent diffusivity, geometry and speed of the meridional flow, dynamo excitation, etc.), computational limitations

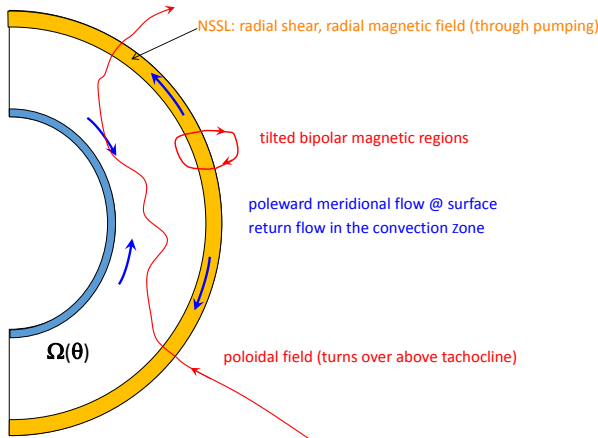


**Fig. 1** Sketch of the updated Babcock-Leighton model of [Cameron and Schüssler \(2017a\)](#).

do not permit a complete coverage of the parameter space. In order to systematically investigate the parameter ranges for solar-like solutions, [Cameron and Schüssler \(2017a\)](#) updated the 1D, two-layer model of [Leighton \(1969\)](#). Model quantities are the azimuthally averaged radial field at the surface and the radially integrated toroidal flux, both as a function of latitude. Poleward meridional flow at the surface, an equatorward return flow somewhere in the convection zone, latitudinal differential rotation as well as radial differential rotation in the near-surface shear layer are included. Furthermore, downward convective pumping of the near-surface horizontal field and turbulent diffusion of the radial surface field and the toroidal field are considered. Using the radially integrated magnetic flux has the advantage that the model neither depends on the radial distribution of the toroidal field in the convection zone nor on the depth location of the meridional return flow. The solutions of this linear model depend on four parameters which represent the driving of the dynamo (by emergence of tilted bipolar regions), the effective speed of the meridional return flow, the turbulent diffusivity affecting the toroidal field in the convection zone, and the effective radial shear below the near-surface shear layer. All other parameters (such as meridional flow and diffusivity at the surface) are taken from observations. The simplicity of the model permits the exploration of the full four-dimensional parameter space. Relevant ranges of parameters are identified by requiring that the model results meet observational constraints: positive growth rate, dipole parity, 22-year magnetic period, flux emergence concentrated in low latitudes, and a 90 deg phase difference between the maximum of flux emergence and maximum strength of the polar field. It turns out that these requirements strongly constrain the parameters, yielding about  $2 \text{ m s}^{-1}$  for the speed of the return flow, a turbulent diffusivity



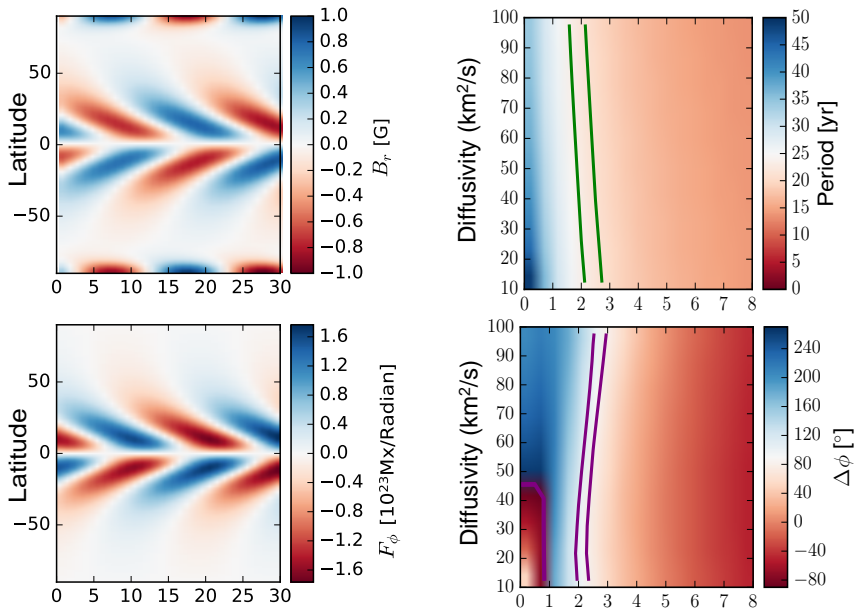


**Fig. 2** Results from the updated Babcock-Leighton model of [Cameron and Schüssler \(2017a\)](#). *Left panels:* Radial surface field (upper panel) and depth-integrated toroidal flux (lower panel) as a function of latitude and time for a solution consistent with the properties of the solar cycle. *Right panels:* Properties of model solutions as functions of the amplitude of the effective speed of the equatorward return flow and of the magnetic diffusivity in the convection zone. Colour shadings indicate the dynamo period (upper panel) and the phase difference between the maximum of the polar field and the maximum rate of flux emergence (lower panel). The regions between the coloured lines indicate “solar-like” models: period in the range 21–23 yr and phase difference between 80 and 100 degrees. These results indicate a rather tight constraint for the speed of the return flow of about  $2\text{--}3\text{ m s}^{-1}$ .

of about  $80\text{ km}^2\text{ s}^{-1}$ , toroidal flux generation dominated by latitudinal differential rotation, and weak dynamo excitation not far above the threshold. A sketch of the model is shown in Fig. 1 and an example of the results in Fig. 2.

The model results of [Leighton \(1969\)](#) indicate that the solar dynamo most probably is a flux-transport dynamo operating near marginal excitation. The model also clearly favors diffusion-dominated dynamo action ([Yeates et al, 2008](#)). The inferred speed of the equatorward flow transporting the toroidal flux is consistent with the latitudinal drift rate of the activity belts. The relevant values of the magnetic diffusivity affecting the toroidal flux are also consistent with the observed evolution of the solar activity belts ([Cameron and Schüssler, 2016](#)). Dominance of latitudinal differential rotation entails a natural explanation for the concentration of flux emergence in low latitudes: the latitudinal rotational shear peaks at mid latitudes and the deep meridional return flow transports the generated toroidal flux equatorward. Consequently,

it is not necessary to assume a threshold value of the toroidal field for the initiation of flux emergence, e.g., in the sense of a buoyancy instability.

Further development of BL dynamo models was provided through a closer connection between the near-surface evolution and the interior evolution of the magnetic field. [Cameron et al \(2012\)](#) found that downward convective pumping (leading to predominantly radial field near the surface) is required to bring a 1D SFT model into accordance with the results of a 2D axisymmetric FTD model (see also [Karak and Cameron, 2016](#)). [Bhowmik and Nandy \(2018\)](#) used the surface distribution of magnetic flux during activity minima resulting from a data-driven SFT simulation as input for a FTD model. A fully coupled 2D×2D model was developed by [Lemerle et al \(2015\)](#) and [Lemerle and Charbonneau \(2017\)](#). These authors connected an observationally calibrated SFT model in latitude and longitude with an axisymmetric FTD model operating in the meridional (radius-latitude) plane. The FTD model provides the source for the SFT model by stochastic flux emergence in tilted bipolar magnetic regions. In turn, the SFT model feeds back upon the FTD model in the form of a BL-like source term near the upper boundary of the dynamo model, resulting in a self-consistent coupling of the two models. [Fig. 3](#) illustrates that properly calibrated results from this model are consistent with the characteristic features of the corresponding solar observations. A similar 2D×2D approach was presented by [Miesch and Dikpati \(2014\)](#).

The BL source in such models is typically provided by “deposition” of tilted bipolar regions in the SFT part of the model, non-locally depending on the strength of the deep-seated toroidal field. This ad-hoc procedure ignores the details of the formation and rise of flux loops through the convection zone, in particular the development of the tilt angle. It also implicitly assumes a dynamical disconnection of the emerged bipolar region from its subsurface roots. [Bekki and Cameron \(2022\)](#) considered the post-emergence evolution of deposited bipolar regions in the framework of a nonlinear 3D simulation in a spherical shell, including the Lorentz force as well as solar-like differential rotation and meridional flow driven by a mean-field prescription. These authors found that the evolution depends sensitively on the initial shape and depth of the injected bipolar regions. When initialized with zero tilt, the Lorentz force in combination with the Coriolis force tends to produce negative tilt angles. The simulated BMRs also develop a systematic asymmetry between the strength of leading and following spots, which is consistent with observations.

[Yeates and Muñoz-Jaramillo \(2013\)](#) suggested a more consistent treatment of flux emergence by assuming helical upflows that transport flux loops through the convection zone, thus capturing aspects of buoyancy and advection by convective flows as well as the connection between the surface and interior field. A similar treatment was proposed by [Pipin \(2022\)](#). The idea of this approach is consistent with the results of detailed observations of the properties of emerging flux, which favor passive flux transport by convective upflows ([Birch et al, 2016](#)). On the other hand, comparison with well-calibrated SFT models ([Whitbread et al, 2019](#)) shows that after emergence the surface flux

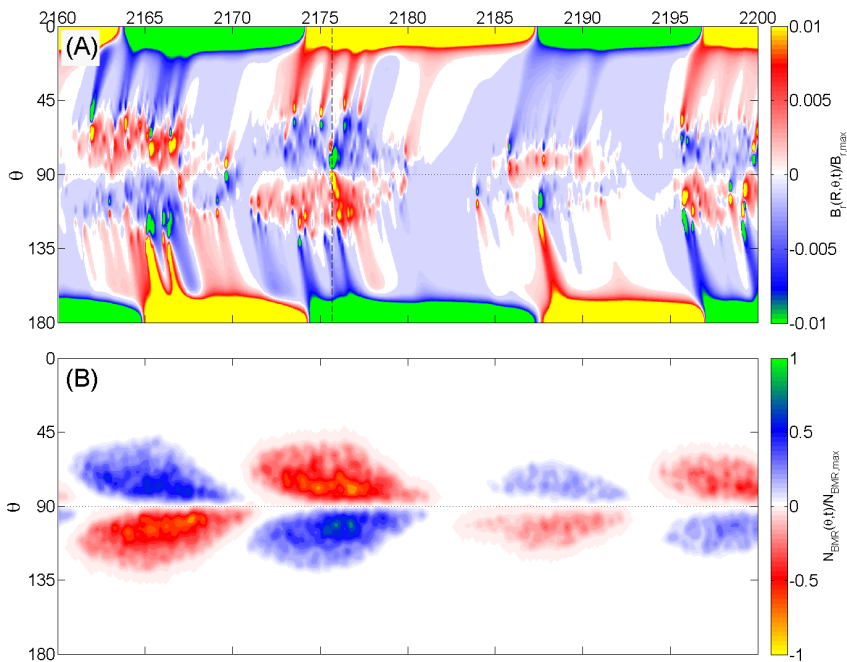


**Fig. 3** Example result obtained by Nagy et al (2017, part of their Fig. 1) using the 2D $\times$ 2D dynamo model developed by Lemerle and Charbonneau (2017). Shown are time-latitude diagrams of the radial field at the surface (upper panel) and of the number of flux emergences (butterfly diagram, lower panel).

needs to be dynamically disconnected from its deep toroidal roots as suggested by Schüssler and Rempel (2005). Moreover, Schunker et al (2019) and Schunker et al (2020) showed that the tilt of bipolar magnetic regions develops only *after* emergence, possibly related to the extended flows converging towards the bipolar magnetic regions (Martin-Belda and Cameron, 2016; Gottschling et al, 2021). In view of these results it seems fair to say that the formation of rising flux loops, their transfer through the convection zone, the actual emergence process, and the subsequent early evolution of the emerged magnetic flux are still poorly understood (see also reviews by Fan, 2021; Isik and etal, 2023), so that these processes cause a significant amount of uncertainty in all FTD/BL models presented so far.

Among the first 3D studies of FTD/BL models for the solar dynamo are the models of Hazra et al (2017) and Karak and Miesch (2017). While these authors used the deposition approach to represent flux emergence, Kumar et al (2019) implemented the more consistent recipe of Yeates and Muñoz-Jaramillo (2013) in a kinematic 3D dynamo code. Another step towards a full 3D treatment was taken by Hazra and Miesch (2018), who introduced a 3D, stationary, convection-like flow field in the upper part of the convection

zone. This serves to replace the diffusion term in standard SFT models by a more realistic explicit transport process. The assumed flow pattern was based upon an observational power spectrum of the surface flows and a downward extrapolation under the assumption of zero divergence of the mass flux and an imposed radial profile. The kinematic model ran into problems owing to unlimited small-scale dynamo action driven by the imposed stationary flow. Further results obtained with kinematic 3D models of BL dynamos have been reviewed by [Hazra \(2021\)](#). [Bekki and Cameron \(2022\)](#) used their 3D model to perform nonlinear BL dynamo simulations with the near-surface deposition of properly tilted bipolar regions. The Lorentz force provides nonlinear saturation of the dynamo amplitude. This feedback drives non-axisymmetric flows as well as solar-like zonal flows superposed upon the differential rotation and also modifies the meridional circulation. Other nonlinear effects (see also Sect. 4.1 that could lead to dynamo saturation and determine the cycle amplitude have been studied by [Jiang \(2020\)](#), [Jiao et al \(2021\)](#), and [Talafha et al \(2022\)](#).

## 3 Generation and removal of magnetic flux

### 3.1 Toroidal flux

Toroidal magnetic field (azimuthal field in the case of an average over longitude) is considered to be generated in the Sun through the action of differential rotation on a poloidal magnetic field. Part of the generated toroidal flux emerges when radial motions carry loops of magnetic flux through the solar surface. Flux emergence leads to the formation of two surface areas with oppositely-directed radial field components. These bipolar magnetic regions (BMRs) have been studied extensively (e.g. [Hale et al, 1919](#); [Harvey et al, 1975](#); [Martin and Harvey, 1979](#); [Wilson et al, 1988](#); [Harvey, 1993](#); [McClintock and Norton, 2016](#); [Schunker et al, 2016](#)). A map showing the latitudes at which larger BMRs with sunspots emerge in time (known as the butterfly diagram) is shown in the upper panel of Fig. 4.

BMRs show various systematic properties. One example is Hale's law ([Hale et al, 1919](#)), which states that the leading polarity (with respect to the direction of rotation) of BMRs in each hemisphere has the same sign in most (up to 95%) of the cases during an activity cycle. The leading polarity is opposite in the two hemispheres and switches from cycle to cycle. These properties imply a systematic East-West component of the horizontal field during emergence, which flips sign between each hemisphere and from cycle to cycle. This can be illustrated in a time-latitude map of the longitudinally averaged azimuthal component of the surface field covering four activity cycles, which is shown in the middle panel of Fig. 4 (cf. [Cameron et al, 2018](#); [Liu and Scherrer, 2022](#)). The latitudes where sunspot groups emerge correspond to locations where the surface azimuthal field is strong. Weaker azimuthal field corresponds to flux emergence of smaller BMRs (ephemeral regions, [Martin and Harvey, 1979](#)).

Another systematic property of BMRs is Joy's law ([Hale et al, 1919](#)). It refers to the tendency for the leading part of a BMR or sunspot group to be

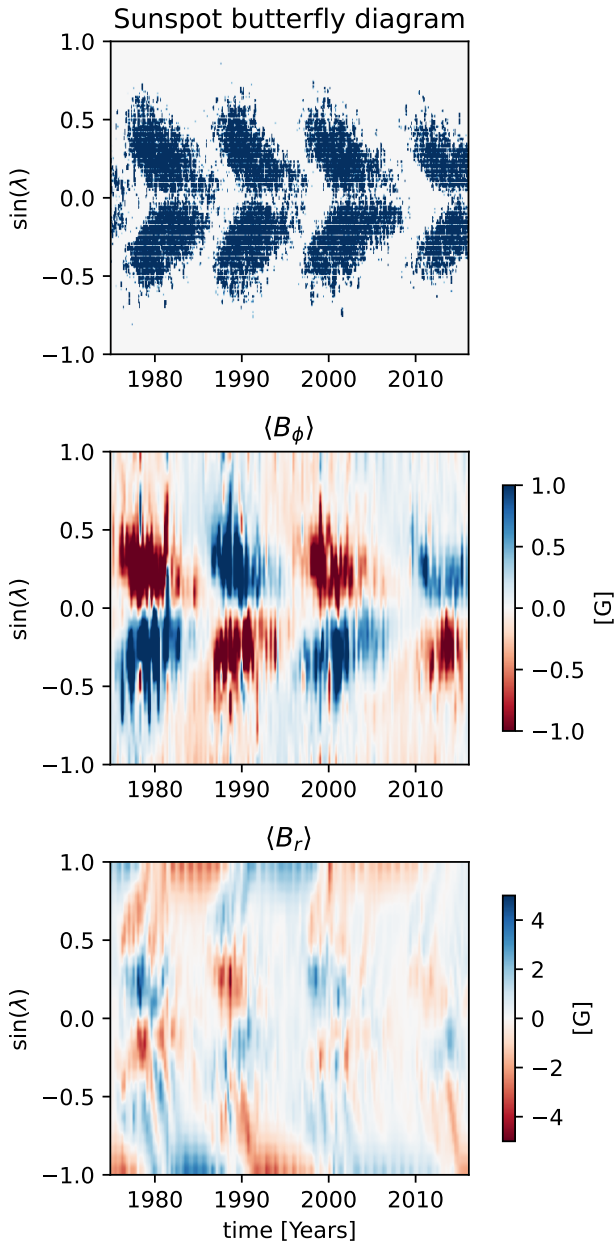


**Fig. 4** Observationally based time-latitude diagrams of sunspots (top panel, data from Royal Greenwich Observatory/NOAA: [http://solarcyclescience.com/AR\\_Database](http://solarcyclescience.com/AR_Database)), longitudinally averaged azimuthal surface field (middle panel, data from Wilcox Solar Observatory, WSO), and longitudinally averaged radial field (lower panel, data from WSO).

closer to the equator. Because of Hale’s law, the leading parts mostly have the same polarity, so that there is a systematic tendency in both hemispheres that more radial magnetic flux of one polarity appears closer to the equator. The radial field of the leading parts in the other hemisphere has the opposite polarity, and the polarities switch from cycle to cycle. These properties are illustrated in the time-latitude diagram for the longitudinally averaged radial surface field shown in the bottom panel of Fig. 4. The locations of flux emergence can be clearly seen, with the leading polarity dominating on the equatorward side of the “butterfly wings”. Plumes of magnetic field with widths of a few months connect the butterfly wings to the polar regions, where the field switches polarity with the period of the solar cycle.

An important feature of the time-latitude diagram of the toroidal surface field (middle panel of Fig. 4) is that during times of activity maximum (when there are many sunspots) the toroidal field at every latitude in each hemisphere is of the same sign. This suggests to consider the evolution of the net subsurface toroidal flux in each hemisphere. For this we start from the induction equation,

$$\frac{\partial \mathbf{B}}{\partial t} = \nabla \times (\mathbf{U} \times \mathbf{B} - \eta \nabla \times \mathbf{B}), \quad (1)$$

where  $\mathbf{B}$  is the magnetic field,  $\mathbf{U}$  the flow velocity, and  $\eta$  the (molecular) magnetic diffusivity. Following Cameron and Schüssler (2015), Cameron and Schüssler (2020), and Jeffers et al (2022), we now consider the area  $A$  that is enclosed by the thick outline in the left panel of Fig. 5 and apply Stokes’ theorem to the induction equation, viz.

$$\frac{\partial \iint_A \mathbf{B} \cdot d\mathbf{A}}{\partial t} = \oint_{\delta A} (\mathbf{U} \times \mathbf{B} - \eta \nabla \times \mathbf{B}) \cdot d\mathbf{l}, \quad (2)$$

where  $\delta A$  indicates the boundary of  $A$  and  $d\mathbf{l}$  is the corresponding line element. We now take the azimuthal average of Eq. (2) and neglect the diffusive term in the contour integral since the magnetic Reynolds number is very large. This leads to

$$\frac{\partial \iint_A \langle \mathbf{B} \rangle \cdot d\mathbf{A}}{\partial t} = \oint_{\delta A} (\langle \mathbf{U} \rangle \times \langle \mathbf{B} \rangle + \langle \mathbf{u} \times \mathbf{b} \rangle) \cdot d\mathbf{l}, \quad (3)$$

where  $\langle \dots \rangle$  indicates the azimuthal average. This equation represents the temporal change of net toroidal flux in the Northern hemisphere resulting from the inductive action of the flow field on the magnetic field. The quantities  $\mathbf{b} = \mathbf{B} - \langle \mathbf{B} \rangle$  and  $\mathbf{u} = \mathbf{U} - \langle \mathbf{U} \rangle$  denote, respectively, the fluctuating components of magnetic field and flow velocity with respect to the corresponding azimuthal averages.

Since the Sun’s radial differential rotation in the equatorial plane is small compared to its latitudinal differential rotation (see right panel of Fig. 5) it is convenient to use a frame of reference rotating with the surface equatorial

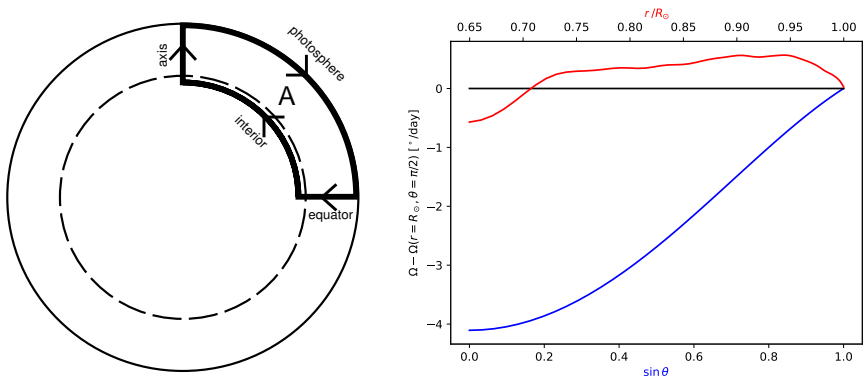


**Fig. 5** *Left panel:* Area and contour used for calculating the net axisymmetric toroidal flux in a hemisphere. The bottom part of the contour is placed at a radius  $R_{\text{interior}}$ , where the penetration of the 22 year cyclic component of the magnetic field is negligible. *Right panel:* Solar differential rotation along segments of the contour in the left panel. Shown are the radial dependence of  $\Omega$  on the equatorial plane (red curve, upper scale) and the (co)latitudinal dependence at the surface (blue curve, lower scale), both relative to the equatorial surface rotation rate. The data for this plot was obtained from [Larson and Chou \(2018\)](#).

rate. In this frame, we have

$$\oint_{\delta A} ((\mathbf{U}) \times \langle \mathbf{B} \rangle) \cdot d\mathbf{l} = \int_0^{\pi/2} \left( \Omega(R_{\odot}, \theta) - \Omega(R_{\odot}, \frac{\pi}{2}) \right) \sin \theta \langle B_r \rangle R_{\odot}^2 d\theta - \int_{R_{\text{interior}}}^{R_{\odot}} \left( \Omega(r, \frac{\pi}{2}) - \Omega(R_{\odot}, \frac{\pi}{2}) \right) \langle B_{\theta} \rangle r dr, \quad (4)$$

where  $\theta$  is the colatitude. Only the surface part of the contour integral (first term on right-hand side) and the part in the equatorial plane (second term) contribute to the contour integral. The bottom part in the interior vanishes since  $\mathbf{B}$  is zero there and the part along the rotation axis vanishes since we consider azimuthal averages of all quantities. The solenoidality of the magnetic field implies

$$\int_0^{\pi/2} \langle B_r \rangle R_{\odot}^2 \sin \theta d\theta = - \int_{R_{\text{interior}}}^{R_{\odot}} \langle B_{\theta} \rangle r dr, \quad (5)$$

which means that the net magnetic flux through the equatorial plane beneath the surface is equal in magnitude to the net flux through the solar surface in each hemisphere.

Owing to the weak radial differential rotation in the equatorial plan), the net toroidal flux generation is strongly dominated by the surface part of the contour integral, i.e., the first term on the right-hand side of Eq. (4). This can be directly evaluated from synoptic observations of the radial field on the surface and the Sun's differential rotation, with a net hemispheric toroidal flux of  $5\text{--}8 \times 10^{23}$  Mx per cycle being thus generated. The integrand for the surface

part in the contour integral (Eq. 4) is strongly dominated by the polar caps (see bottom left panel of Fig. 6), so that the flux associated with the polar dipole field represents the relevant poloidal source for the generation of net toroidal flux. Other poloidal flux that is contained in the convection zone and does not cross the surface leads to equal amounts of East-West and West-East orientated toroidal flux in a hemisphere and thus does not contribute to the net toroidal flux required by Hale’s polarity laws.

The term in Eq. 3 involving the fluctuating components,  $\oint_{\delta A} \langle \mathbf{u} \times \mathbf{b} \rangle \cdot d\mathbf{l}$ , is dominated by (turbulent) diffusive fluxes across the axis and the equatorial plane. Some of the other terms, such as those owing to the turbulent electromotoric force ( $\alpha$ -effect), are expected to vanish due to symmetries – along the axis owing to the conservation of helicity and at the equator owing to the expected vanishing of the kinetic helicity, which in its simplest form scales like  $\cos \theta$ .

Another contribution from the fluctuating terms is the change of the net toroidal flux by flux emergence and submergence through the surface, which is described by

$$\left( \frac{d\Phi}{dt} \right)_{\text{em,subm}} = \int_{\pi/2}^0 \langle u_r b_\phi \rangle |_{R_\odot} R_\odot d\theta. \quad (6)$$

Flux loss through the surface was part of the original Babcock-Leighton model (Leighton, 1969), but later fell out of favour since it was thought that the emerged flux is mostly retracted back through the surface (e.g., Wallenhorst and Topka, 1982). This process can take place in flux cancellation events when loops of emerged flux become sufficiently narrow, so that the tension force dominates. Some retraction of flux is possibly required to account for the amount of flux brought to the surface by repeated emergences in so-called “nests of activity” (e.g., Gaizauskas et al, 1983).

Parker (1984) argued that a net loss of toroidal flux from the Sun would require an organized sequence of reconnection events between narrowly-spaced bipolar regions, thus effectively shedding the mass from the toroidal field lines and allowing them to freely escape with the solar wind. However, observations show that the bipolar regions generally are much too widely spaced for this process to operate on the Sun, so that Parker concluded that in dynamo models the solar photosphere should be approximated by an impenetrable boundary.

Parker’s argument, however, ignores that what is relevant for the dynamo models is the effect of the emergence on the *mean* (azimuthally averaged) toroidal field. Cameron and Schüssler (2020) showed that the amount of the azimuthally averaged toroidal field lost due to the emergence of a bipolar region is time-independent, irrespective of the further evolution of its magnetic flux. While cancellation/retraction of most of the field may occur, at the same time the remaining surface flux spreads out in longitude (transported by near-surface flows) to eventually fully encircle the Sun. In this way, toroidal field detached from the solar interior is formed which can be carried away by the solar wind and the same amount of flux is lost from the mean toroidal field in the interior. A quantitative analysis of the net azimuthally averaged toroidal



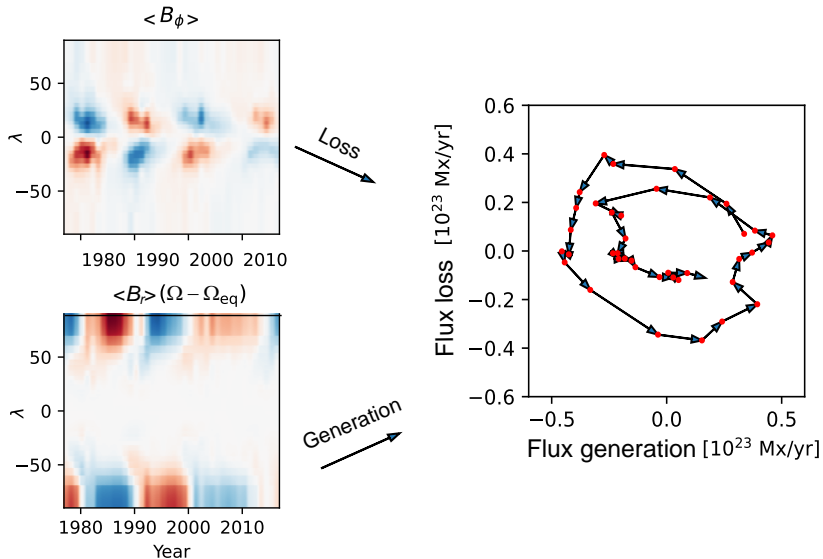


**Fig. 6** Generation and loss of net unsigned toroidal flux in the Northern hemisphere, covering four activity cycles on the basis of synoptic magnetograms from the Wilcox Solar Observatory. The time-latitude diagrams on the left side show the observational input for evaluating the dominating surface part of the contour integral (Eqs. 4 and 6). Toroidal flux is generated proportional to the product of the azimuthally averaged surface radial field and the surface rotation rate relative to the equatorial rate (lower left panel). Toroidal flux is lost through flux emergence at a rate proportional to the product of  $\langle B_\phi \rangle$  at the surface (upper left panel) and the radial emergence velocity estimated as  $v_{em} = 200 \text{ m s}^{-1}$  (Cen-teno, 2012). The panel to the right shows a phase plot of the yearly integrated values of the generated and lost toroidal flux indicated by red dots. The connecting line segments with arrows illustrate the change from one year to the next.

flux lost during a cycle arrives at  $3.3 \times 10^{23} \text{ Mx/hemisphere/cycle}$  (Cameron and Schüssler, 2020). A similar estimate of  $5 \times 10^{23}$  was obtained using in situ measurements of the magnetic field and flows in the solar wind (Bieber and Rust, 1995). The observations thus indicate that, integrated over a cycle, the amount of the toroidal magnetic flux generated by the axisymmetric flows and fields ( $\oint_{\delta A} \langle \mathbf{U} \times \mathbf{B} \rangle \cdot d\mathbf{l}$ ) is similar to the amount lost through flux emergence ( $\oint_{\delta A} \langle \mathbf{u} \times \mathbf{b} \rangle \cdot d\mathbf{l}$ ).

The toroidal flux budget shown in Figure 6 shows the approximate balance between the amount of toroidal magnetic flux lost throughout a cycle due to flux emergence and the amount produced by the winding up of poloidal flux threading the solar surface, both being determined by surface observations of the magnetic field ( $B_\phi$  and  $B_r$ ). There is a phase shift between the production rate and loss of about  $90^\circ$ , which is consistent with the loss through flux emergence being proportional to the total subsurface toroidal flux. The phase diagram is based on Eqs. (4) and (6), which confirms the concept that the toroidal flux is mainly generated by the action of latitudinal differential rotation on the poloidal flux threading the solar surface in the polar dipole field.

### 3.2 Poloidal flux

The previous section has shown that the application of Stokes' theorem to the induction equation over a properly defined meridional area illuminates the essence of the generation and loss of net toroidal flux during solar activity cycles. A similar procedure can be used to determine the evolution of the net radial flux threading a hemisphere of the Sun (cf. [Durrant et al, 2004](#)). To this end, we integrate the radial component of the azimuthally averaged induction equation over the photospheric surface area,  $A$ , of the Northern hemisphere, NH, and apply Stokes' theorem, which yields

$$\frac{\partial \Phi_{\text{pol,NH}}}{\partial t} = \frac{\partial}{\partial t} \oint_A B_r dA = 2\pi R_\odot (\langle u_r b_\theta \rangle - \langle u_\theta b_r \rangle), \quad (7)$$

where the contour integral is taken over the boundary of  $A$ , i.e., the equator. The two terms on the r.h.s. correspond to observable quantities. The term  $\langle u_r b_\theta \rangle$  quantifies the effect of flux emerging across the equator. This term is important when large and highly tilted active regions emerge with polarities on either side of the equator (e.g., [Cameron et al, 2013](#)). The term  $\langle u_\theta b_r \rangle$  corresponds to convective motions carrying radial flux across the equator and can be approximated by a "turbulent" diffusion term, viz.

$$\langle u_\theta b_r \rangle = \eta_T R_\odot \frac{\partial B_r}{\partial \theta}. \quad (8)$$

There is a systematic component to  $\partial B_r / \partial \theta$  corresponding to the systematic tilt angle of bipolar regions (see the time-latitude diagram of the radial magnetic field in [Fig. 4](#)). A random component is introduced by large, highly tilted active regions which emerge near to the equator ([Cameron et al, 2013](#)), also called "rogue active regions" ([Nagy et al, 2017](#)). Such regions introduce significant randomness into the net flux in each hemisphere and the axial dipole moment ([Cameron et al, 2014](#)). This randomness thus carries over into the production of the toroidal flux emerging in the subsequent cycle. [Jiang et al \(2015\)](#) and [Whitbread et al \(2018\)](#) showed that the low amplitude of solar cycle 24 can be understood in terms of rogue active regions that emerged during cycle 23.

[Figure 7](#) illustrates the budget of poloidal surface flux for four activity cycles on the basis of synoptic magnetograms from the Wilcox Solar Observatory. The poloidal flux is determined by integration of the longitudinally averaged radial field over the solar surface, viz.

$$\Phi_{\text{pol}} = \pi R_\odot^2 \int_0^\pi \langle B_r \rangle \text{sign}(\pi/2 - \theta) \sin \theta d\theta, \quad (9)$$

where the results for the two hemispheres are averaged.

The generation term for the poloidal flux results from summing the contributions of all bipolar regions to the amount of magnetic flux which is carried

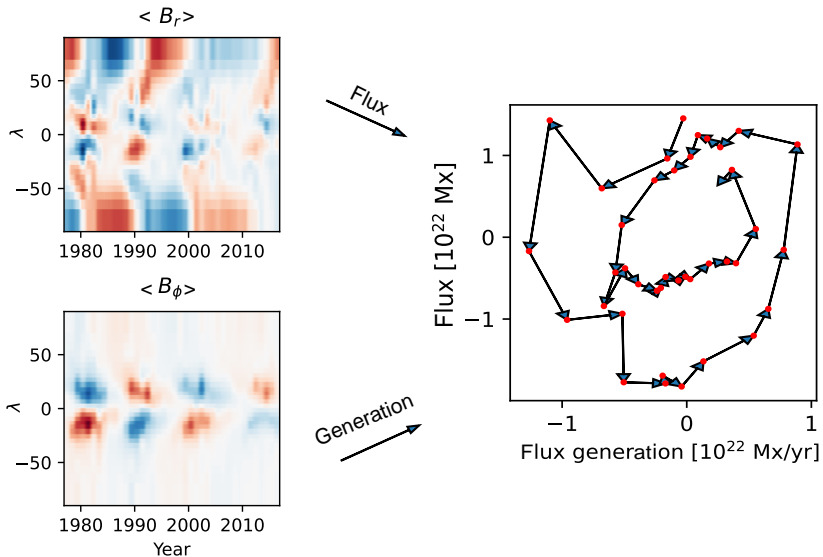


**Fig. 7** Systematic part of the generation rate and amount of net poloidal flux in the course of four activity cycles. The left panels illustrate the observational input: the azimuthally averaged radial surface field (upper left panel) determines the total net poloidal surface flux (cf. Eq. 9) while the azimuthally averaged azimuthal surface field (lower left panel) represents flux emergence in tilted bipolar regions and thus determines the rate of generation of poloidal flux via flux transported over the equator (cf. Eq. 15). The right panel shows a phase plot of both quantities, with each red dot representing the the average value for one year. The line segments with arrows represent the change from one year to the next.

across the equator. The contribution of a single bipolar region ( $i$ ) depends on the magnetic flux of each polarity,  $\Phi_i$ , the angular separation of the two polarities in latitude,  $\delta_{\lambda,i}$ , the latitude of emergence,  $\lambda_i$ , and a parameter characterizing the surface evolution of the magnetic flux near the equator,  $\lambda_R$  (cf. Petrovay et al, 2020). This parameter depends on the latitudinal derivative of the surface meridional flow speed,  $V$ , at the equator ( $\lambda = 0$ ), and the turbulent diffusivity at the surface,  $\eta_T$ , viz.

$$\lambda_R = \sqrt{\frac{\eta_T}{R_\odot (dV/d\lambda)_{\lambda=0}}}. \quad (10)$$

Petrovay et al (2020) estimated the time-integrated amount of magnetic flux crossing the equator (and thus the contribution of the bipolar region to the buildup of the poloidal field) by the leading term of a Taylor expansion as

$$\Phi_{\text{pol},i} = \frac{\Phi_i \delta_{\lambda,i}}{\sqrt{2\pi} \lambda_R} e^{-\lambda_i^2 / (2\lambda_R^2)}. \quad (11)$$

During its emergence, the flux tube forming the bipolar region contributes to the longitudinally averaged toroidal surface field,  $\langle B_\phi \rangle$ , by the amount  $\langle B_{\phi,i} \rangle$

according to

$$\Phi_i \frac{\delta_{\phi,i}}{2\pi} = \langle B_{\phi,i} \rangle v_{\text{em}} \Delta t R_{\odot} \Delta \lambda, \quad (12)$$

where  $\delta_{\phi,i}$  is the longitudinal angular extent of the bipolar region,  $\Delta t$  is the time over which the emergence takes place,  $\Delta \lambda$  is the latitudinal width of the leading polarity of the emerging region, and  $v_{\text{em}}$  is the mean emergence speed (assumed to be the same for all emergences). The latitudinal and longitudinal extents are related by  $\delta_{\lambda,i} = \tan(\alpha_i) \cos(\lambda_i) \delta_{\phi,i}$ , where  $\alpha_i$  is tilt angle. We thus obtain

$$\Phi_i \delta_{\lambda,i} = \langle B_{\phi,i} \rangle v_{\text{em}} \Delta t R_{\odot} \Delta \lambda 2\pi \tan(\alpha_i) \cos(\lambda_i). \quad (13)$$

Inserting this result into Eq. (11), we obtain

$$\Phi_{\text{pol},i} = \frac{\langle B_{\phi,i} \rangle v_{\text{em},i} \Delta t R_{\odot} \Delta \lambda \sqrt{2\pi} \tan(\alpha_i) \cos(\lambda_i)}{\lambda_R} e^{-\lambda_i^2/(2\lambda_R^2)} \quad (14)$$

For the the tilt angle we consider Joy's law without scatter, so that  $\alpha_i = \alpha(\lambda_i)$ . We further assume that the emergence velocity is the same for all bipolar regions with a value of  $v_{\text{em}} = 200 \text{ m s}^{-1}$  (Centeno, 2012). Adding together the contributions of the individual bipolar regions to obtain the rate of generation of poloidal flux then amounts to the latitude integral

$$\frac{d\Phi_{\text{pol}}}{dt} = \frac{\sqrt{2\pi} v_{\text{em}}}{\lambda_R} \int_{-\pi/2}^{\pi/2} \langle B_{\phi} \rangle R_{\odot} \tan[\alpha(\lambda)] \cos(\lambda) e^{-\lambda^2/(2\lambda_R^2)} d\lambda \quad (15)$$

We choose the parameters as in Jiang et al (2014a) with  $\eta_{\Gamma} = 250 \text{ km}^2\text{s}^{-1}$ , surface meridional flow  $V(\lambda) = 11 \sin(180\lambda/75) \text{ m s}^{-1}$ , and Joy's law for a cycle of intermediate strength in the form  $\alpha(\lambda) = 0.7 \times 1.3 \sqrt{|\lambda|} \text{ sign}(\lambda)$ .

The poloidal flux budget resulting from using the observed longitudinally averaged radial and azimuthal surface fields in Eqs. (9) and (15) is illustrated by the phase diagram on the right side of Figure 7. It demonstrates that poloidal flux and poloidal flux generation as determined through Eqs. (9) and (15) are consistent with each other. This confirms the basic concept that the poloidal field is being generated by the joint contributions of tilted bipolar regions. Compared to the toroidal flux budget (Figure 6), the phase diagram is somewhat less smooth. This is a consequence of the significant random component affecting the generation of poloidal flux. This component is only included in the poloidal flux but not in the rate of poloidal flux generation, where we have assumed Joy's law without scatter.

### 3.3 Flux transport

The net toroidal and poloidal flux budgets discussed in the previous sections show that the observable magnetic flux at the surface plays a crucial role in the solar dynamo, highlighting the role of differential rotation, flux emergence, and Joy's law. This section briefly discusses additional processes which modify the spatial distribution of the fluxes. In terms of the poloidal flux, the budget

shown in Fig. 7 demonstrates that flux carried across the equator is essential. Furthermore, the toroidal flux budget is dominated by the polar fields, which means that the poleward transport of flux is an important ingredient of the dynamo process: surface flux which crosses the equator is transported to the poles by a combination of the large-scale meridional flow and small-scale flows associated with convection. These processes are captured by the surface flux transport model (Jiang et al, 2014b; Yeates et al, 2023).

The butterfly diagram of flux emergence demonstrates that there is a similar requirement for the equatorward transport of the subsurface toroidal flux from latitudes of about  $55^\circ$ , where the toroidal flux is most efficiently produced (cf. Spruit, 2011), towards the equator. Low-latitude flux emergence in accordance with Joy's law then leads to the cross-equatorial transport of poloidal field. The nature of this transport of toroidal flux is not directly constrained, so that dynamo waves, turbulent pumping, and meridional circulation are all viable candidates. Gizon et al (2020) showed that the speed of the deep equatorward meridional flow inferred from helioseismology is consistent with the observed migration of the activity belts if the toroidal flux is distributed over the lower half of the convection zone. This lends credibility to the concept of flux transport dynamos (recently reviewed by Hazra et al, 2023).

## 4 Nonlinearity, predictability, and long-term variability

### 4.1 Nonlinear effects

An excited hydromagnetic dynamo leads to exponential growth of an initially weak magnetic field until further amplification becomes limited by the action of the Lorentz force, which introduces a nonlinearity into the system. The nonlinearity can affect large-scale flows (e.g, differential rotation and meridional flow), modify turbulence effects (e.g., the mean-field  $\alpha$ -term, turbulent diffusivity, and turbulent pumping), or change the properties of flux emergence. A nonlinearity often invoked in mean-field models is “ $\alpha$ -quenching” (Steenbeck and Krause, 1969; Stix, 1972), a parameterization of the decreasing efficiency of turbulence to produce poloidal field from the toroidal field as the field amplitude grows. In the case of a system with a high magnetic Reynolds number,  $R_m$ , such as the Sun, this nonlinearity is potentially catastrophic since the ratio of the small-scale field and the mean field scales as  $\sqrt{R_m}$  (Cattaneo and Vainshtein, 1991). This causes saturation of the dynamo at field amplitudes many orders of magnitude smaller than observed on the Sun. However, catastrophic quenching may be alleviated by removal of magnetic helicity from the system (Kleeorin et al, 2000; Hubbard and Brandenburg, 2012).

In the Babcock-Leighton framework, the poloidal field generation results from the systematic tilt angle of bipolar magnetic regions. While there is observational evidence that the average tilt angle decreases with increasing cycle strength (Dasi-Espuig et al, 2010; McClintock and Norton, 2013; Jiao et al,

2021), catastrophic quenching is not expected in this case (Kitchatinov and Olemskiy, 2011a). Sufficiently strong magnetic field may also reduce the turbulent magnetic diffusivity (e.g., Kleeorin and Rogachevskii, 2007; Guerrero et al, 2009), which also affects the Babcock-Leighton dynamo.

Magnetically induced changes of the large-scale differential rotation (zonal flows, cf. Labonte and Howard, 1982) and of the meridional circulation (systematic inflows towards active regions, cf. Gizon et al, 2001) have been observed (see also Hathaway et al, 2022). The zonal flows are probably too weak to have a substantial effect on the dynamo mechanism. The inflows towards active regions explain part of the cyclic variation of the meridional flow (Cameron and Schüssler, 2012). Their effects have been studied in the framework of surface flux transport and Babcock-Leighton models (Martin-Belda and Cameron, 2017; Nagy et al, 2020). It was found that, in principle, the resulting changes to the meridional flow can provide nonlinear saturation of the dynamo.

Another nonlinearity which has been studied in the Babcock-Leighton framework is ‘latitudinal quenching’ (Jiang, 2020; Talafha et al, 2022). This effect is related to the observation that the average latitudes of sunspots are located more poleward in strong cycles as compared to weak cycles (Waldmeier, 1955; Solanki et al, 2008; Hathaway, 2015). Since bipolar regions at higher latitudes contribute less to the flux crossing the equator and thus to the buildup of the poloidal field (Jiang et al, 2014a), this effect provides an amplitude-limiting nonlinearity.

A closer look at the properties of flux emergence depending on cycle strength yields further insight into the nature of latitude quenching. In Fig. 8, we used 13-month smoothed sunspot numbers (Version 2) between solar cycles 12 and 24 from the SILSO data base (<https://www.sidc.be/silso/datafiles>) and 12-month averages of observed times, latitudes, and areas of sunspots given in the Royal Greenwich Observatory and USAF/NOAA data bases (downloaded from <http://solarcyclescience.com/activerregions.html>) to plot the sunspot number, the central latitude, and the full width at half maximum (FWHM) of the sunspot zones (“butterfly wings”), respectively, as functions of time since the start of a cycle. Depending on their peak sunspot number, four cycles each were put into groups of strong, medium, and weak cycles. Central latitude and FWHM of the sunspot zones were determined from Gaussian fits of the sunspot data with unsigned latitudes, thus merging both hemispheres.

Since the solar cycle is not perfectly periodic, comparing the evolution of different cycles requires a definition of a reference time for each cycle. One possibility is to fit the shape of the time evolution of the sunspot number to a given functional relationship. Using such a procedure, Hathaway (2011) found that the central latitude of the sunspot belts propagates equatorward in the same way for all cycles (see also Waldmeier, 1939). We thus take the reference time as the instant at which the central latitude is at  $19^\circ$  and define the start of the cycle to be 4 years before that instant. These particular choices have no significant impact on the analysis and the results.

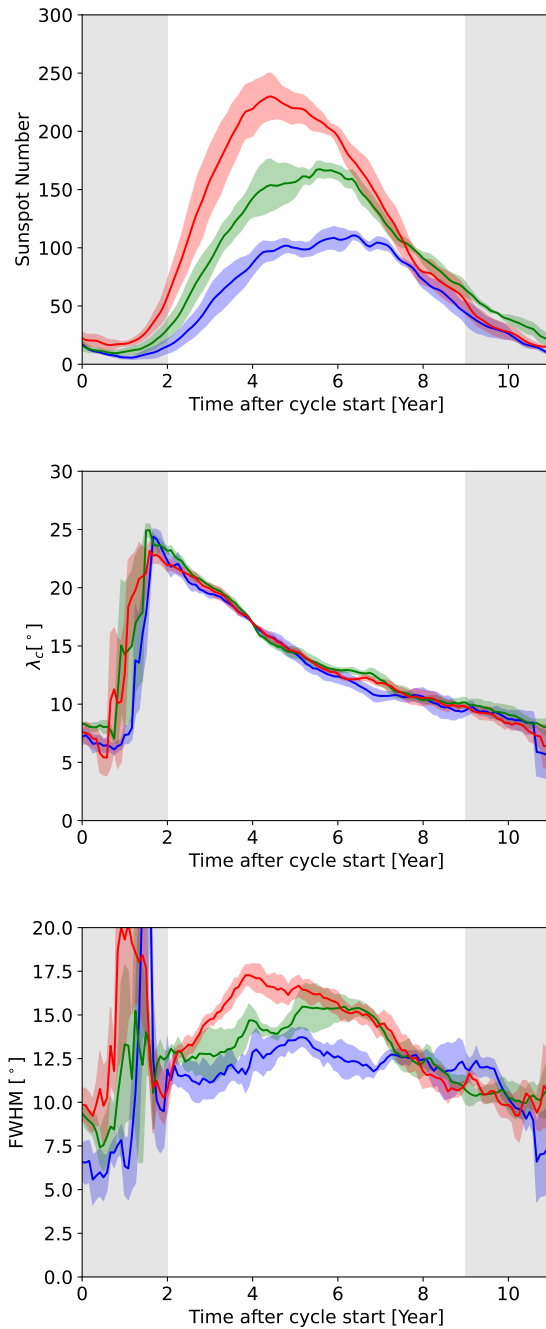


**Fig. 8** Properties of the sunspot zones as function of time from cycle start, based upon the historical sunspot record. Shown are the sunspot number (top panel), central latitude (middle panel), and full width at half maximum (lower panel) of the sunspot zones. The quantities are averaged over weak cycles ( $n = 12, 14, 24, 16$ , blue lines), intermediate cycles ( $n = 15, 20, 17, 23$ , green lines), and strong cycles ( $n = 18, 21, 22, 19$ , red lines). Shading indicates the range covered by the  $\pm 1$  stderr, calculated using the scatter between the four cycles in each group.

The figure confirms earlier results of [Waldmeier \(1955\)](#): (i) the activity of stronger cycles rises faster and peaks earlier than that of weaker cycles (often referred to as “Waldmeier effect”) while the declining phase is independent of cycle strength, and (ii) the time profile of the propagation of the sunspot zones towards the equator is independent of cycle strength (see also [Hathaway, 2011](#)). Furthermore, the full width at half maximum of the sunspot zones in the declining phase is also independent of cycle strength ([Cameron and Schüssler, 2016](#)), while stronger cycles show broader sunspot zones (see also [Mandal et al, 2017](#); [Biswas et al, 2022](#)). These properties reveal three aspects of latitude quenching, namely

1. The Waldmeier effect has the consequence that flux emergence around cycle maxima on average occurs in higher latitudes for stronger cycles than for weaker cycles, thus being less effective for the buildup of the polar field. This corresponds to a negative feedback.
2. The broader wings of the sunspot zones during the maximum phases of stronger cycles have the opposite effect since more flux emerges in lower latitudes.
3. The fact that all three properties, sunspot number as well as central latitude and width of the sunspot zones, behave independently of cycle strength in the declining phase of the cycles means that, during this most critical phase for the buildup of the poloidal field, the amount of magnetic flux transfer transferred across the equator is independent of cycle strength, thus corresponding to negative feedback.

These three aspects reveal the action of an underlying nonlinearity connected to flux emergence. It is plausible that the cycle strength reflects the amount of toroidal magnetic flux in the convection zone which is available for flux emergence. In strong cycles, latitudinal differential rotation, which is steepest in mid latitudes, acts upon a stronger poloidal field and thus produces more and stronger toroidal magnetic flux. A nonlinearity matching the cycle properties discussed above could be that flux emergence occurs when a critical field strength of the order of the equipartition field strength is exceeded. While the latitude drift of the sunspot zones is independent of cycle strength (possibly being determined by a deep meridional flow towards the equator, which is largely unaffected by the magnetic field), the critical field strength is reached earlier in strong cycles, meaning that more flux emerges at higher latitudes (point 1 of the list above). At the same time, the critical field strength is exceeded in a broader range of latitudes (point 2). Consequently, stronger cycles have lost a bigger part of their available toroidal flux earlier in the cycle compared to weaker cycles, so that in the later phases flux emergence and width of the sunspot zones become independent of cycle strength. [Biswas et al \(2022\)](#) confirmed this conjecture using a Babcock-Leighton flux-transport dynamo model. They suggested that, in the declining phase of all cycles, flux emergence compensates the increase of the toroidal field strength due to the pileup of flux near the stagnation point of the equatorward meridional flow.



Consequently, the mean field strength remains near to the critical field strength for flux emergence and all cycles decline in the same way.

All mechanisms discussed in this section are plausible explanations for the nonlinearity limiting the amplitude of the solar dynamo. Distinguishing which combination of them acts on the Sun is an open observational challenge.

## 4.2 Long-term variability

The sunspot cycle shows variability on a wide range of timescales (see reviews by [Usoskin, 2017](#); [Biswas et al, 2023](#)). Panel A of Fig. 9 shows the historical sunspot record from telescopic observations since the beginning of the 17th century. It reveals significant cycle-to-cycle fluctuations of cycle strength together with longer-term variability. Particularly conspicuous is the period of very low sunspot activity between 1645 to 1715 and the period of high average sunspot activity between about 1940 and 2006. Other such “grand minima” and “grand maxima” are found in reconstructions of solar activity during the past millenia (albeit at a coarser time resolution) on the basis of various records of cosmogenic isotopes (e.g., [Solanki et al, 2004](#); [Usoskin et al, 2016](#)). An example of such a reconstruction is shown in panel B of Fig. 9.

Observational studies of the rotational evolution (gyrochronology) of solar-type stars (e.g., [Metcalf et al, 2016](#); [van Saders et al, 2016](#); [David et al, 2022](#); [Metcalf et al, 2022, 2023](#)) indicate that magnetic braking by a stellar wind is significantly reduced for stars near or beyond the solar age, which suggests a decline of their large-scale magnetic fields (for a different view, see [Kotorashvili et al, 2023](#)). This indicates that, at its current rotation rate, the Sun could be approaching a transition point where its global dynamo switches off, so that at present the excitation of the solar dynamo is only weakly supercritical (or even subcritical, as suggested by [Tripathi et al, 2021](#)).

The observationally well-studied rotation-activity relation for magnetically active stars (e.g., [Brun and Browning, 2017](#)) suggests the rotation rate as the relevant control parameter for dynamo excitation. For most dynamo models, the transition from decaying field to excited oscillatory dynamo action corresponds to a supercritical Hopf bifurcation (e.g., [Tobias et al, 1995](#)), when a fixed point (equilibrium) spawns a limit cycle (oscillatory solution). The behaviour of a weakly excited nonlinear system near a Hopf bifurcation is fully described by a generic normal-form model that is independent of the specific properties of the system, including also the nature of its nonlinearity (e.g., [Guckenheimer and Holmes, 1983](#)).

[Cameron and Schüssler \(2017b\)](#) applied this concept to the solar dynamo and showed that the observed power spectrum of the solar cycle (from the sunspot record and from the reconstruction based on cosmogenic isotopes) is consistent with a noisy normal-form model whose parameters are completely determined by observations. The noise in the system results from the large scatter in the observed tilt angles of active regions, which is possibly associated with the interaction of magnetic flux and convective motions ([Longcope and Fisher, 1996](#)). As discussed in Sections 3.1 and 3.2, the tilt angle scatter leads

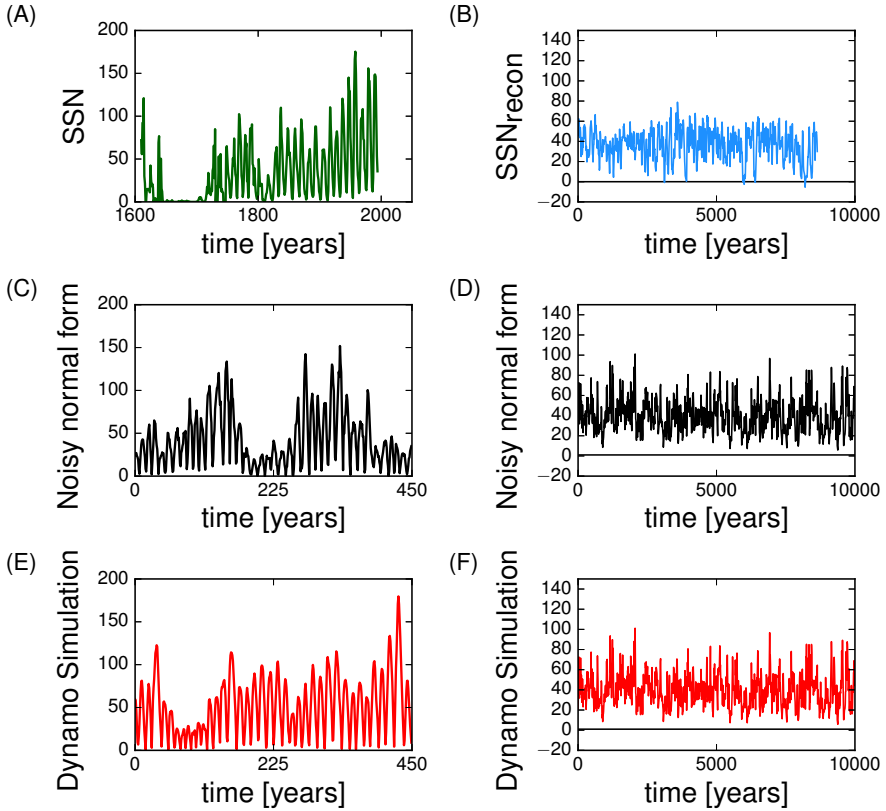


**Fig. 9** Observed and simulated records of solar activity. The historical sunspot record (sunspot group number, panel A) and the level of solar activity reconstructed from cosmogenic isotopes samples (Usoskin et al, 2016) are shown in panels A and B, respectively. Panels C and D in the middle show random realizations of a normal-form model (near a Hopf bifurcation) model with noise, covering the same lengths of time as panels A and B. Panels E and F at the bottom shows realizations from a simple Babcock-Leighton dynamo model. Figure taken from Cameron and Schüssler (2017b).

to randomness in the amount of flux transported across the equator, and hence to randomness in the amount of toroidal field generated for the subsequent cycle.

Panels C and D of Fig. 9 show an example realization of the normal-form model covering 10,000 years. Panel B of Fig. 10 gives the corresponding temporal power spectrum, which is consistent with the observed spectrum shown in panel A of Fig. 10. Moreover, the model also exhibits extended periods of low activity (grand minima) whose statistical properties in terms of the distributions of their lengths and the waiting times between grand minima

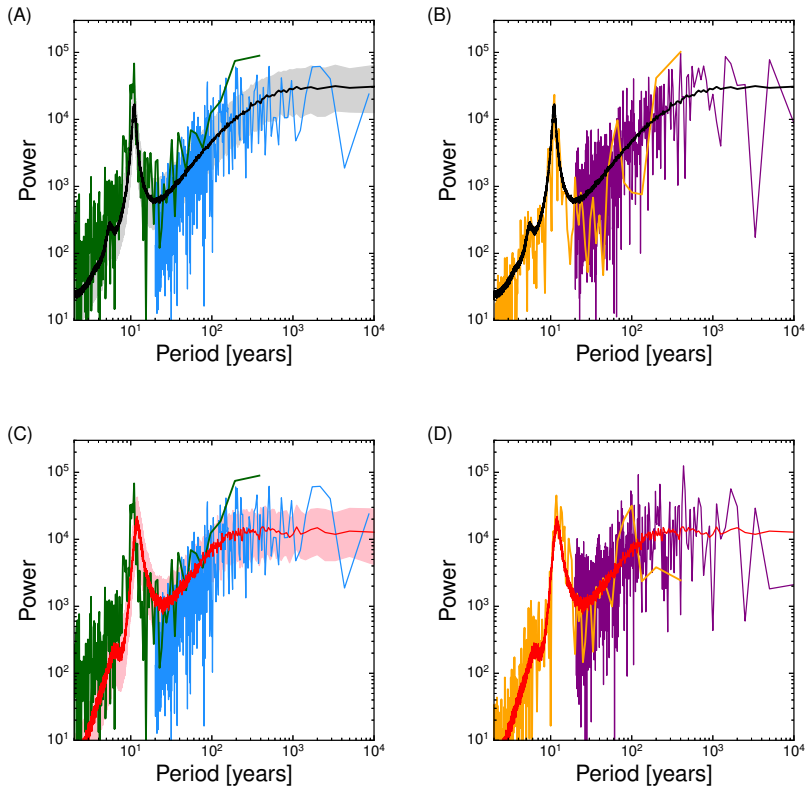


**Fig. 10** Power spectra of empirical solar data and models. (A) Sunspot group number (green), and reconstruction from cosmogenic isotopes (blue), together with the expectation value from 10,000 realizations of the normal form model (black curve) and the corresponding 25% to 75% quartiles (grey shading). (B) One realization of the normal form model. (C) Same as (A), but compared to the expectation value and quartiles from realizations of an updated Babcock-Leighton model (black curve and pink shading). (D) One realization of the updated Babcock-Leighton model. Figure taken from [Cameron and Schüssler \(2017b\)](#).

is consistent with the reconstructed record of solar activity by [Usoskin et al \(2016\)](#).

Likewise, the updated 1D Babcock-Leighton dynamo model of [Cameron and Schüssler \(2017a\)](#) with slightly supercritical excitation and including noise in the source term for the poloidal field also yields time series that are statistically similar to the empirical series (see panels E and F of Fig. 9). The corresponding power spectra in panels C and D of Fig. 10) show a good match to the observed spectra (panel A of Fig. 10). A similar approach was taken by [Kitchatinov and Nepomnyashchikh \(2017\)](#) and [Kitchatinov et al \(2018\)](#), who studied a more comprehensive dynamo model.

Cameron and Schüssler (2019) carried out a detailed analysis of power spectra obtained with the generic noisy normal-form model (incorporating only the 11/22 year base period) in order to evaluate the statistical significance of periodicities inferred from the record of reconstructed solar activity on the basis of cosmogenic isotopes. They showed that power spectra from realizations covering 10,000 years of simulated time (matching the length of the reconstructed solar data) typically exhibit spectral peaks at various periods that are qualitatively similar to those found in the solar data. Such peaks, which result from the stochastic noise in the dynamo excitation, can reach significance levels of  $3\sigma$ . These results cast doubt on the proposition that seemingly significant periodicities such as the 90-year Gleissberg and the 210-year de Vries “cycles” are intrinsic to the solar dynamo and not just statistical fluctuations. In fact, the sharpness of the corresponding peaks in the power spectrum indicates a random origin since spectral peaks representing intrinsic dynamo periodicities tend to be broadened owing to the damping inherent to the dynamo process.

Apart from stochastic forcing as discussed above, long-term variability in the dynamo process can also arise from magnetic feedback on the flow and from time delays in the dynamo process. A comprehensive review of models for the long-term variability has been provided by Karak (2023).

### 4.3 Notes on predictability

Based on sufficient understanding of the global solar dynamo, the observed state of the solar magnetic field can be used to predict its future evolution (for comprehensive reviews, see Petrovay, 2020; Bhowmik et al, 2023). In the Babcock–Leighton model, the cycle-to-cycle variability is directly related to the amount of magnetic flux that gets across the equator. At the end of a cycle, all this flux ends up in the polar regions and the amplitude of the polar field is strongly correlated with the strength of the subsequent cycle (e.g., Kumar et al, 2021). The physical basis for this correlation is explained in Sec. 3.1. Predicting the strength of a cycle thus becomes a matter of predicting the polar field strength at the end of a cycle, which is almost equivalent to predicting how much flux is transported across the equator (see Sec. 3.2). This can be achieved by performing surface-flux-transport simulations using the actual observations of latitude, magnetic flux, and tilt angle of each emerging active region. Such simulations rather accurately reproduce the amount of flux in each hemisphere and the resulting axial dipole moment as a predictor for the subsequent cycle (Jiang et al, 2015; Yeates et al, 2023). A prediction for the next cycle during an ongoing cycle (i.e., before all the active regions of the cycle have emerged) can be made by including all active regions which have been observed and performing Monte-Carlo simulations of the effect of the active regions which have not yet emerged, using their average properties (Cameron et al, 2016). The result of this approach is the prediction of the polar field at the end of the cycle with error estimates. These can then be converted into predictions for the strength of the subsequent cycle.

In any case, all predictions are limited by the inherent randomness of the dynamo process (Jiang et al, 2018; Kitchatinov et al, 2018). For instance, individual “rogue active regions” can have a strong effect and may potentially even shut down the the large-scale dynamo and initiate a grand minimum episode (Nagy et al, 2017).

## 5 Outlook

Considering the enormous range of scales and the complexity of physical processes governing the interaction of turbulent convection, differential rotation, and magnetic field in the solar convection zone, it is rather surprising that a comparatively simple approach such as the Babcock-Leighton scenario seems to provide such a successful description of the solar dynamo process. An important factor here is that key ingredients of the model, such as the properties of bipolar magnetic regions (latitude range, tilt, flux distribution, etc.) and surface flows, can be obtained by observations. To a large extent, such observations are not available for other stars, so that basic input is missing for the application of the model. Furthermore, the underlying processes leading to flux emergence, i.e., the roles of convective flows, magnetic buoyancy, and instabilities deep in the convection zone, are largely not understood. In the absence of direct observational evidence, 3D MHD simulations seem to be the only possibility here. Considering the impressive progress that simulations have seen during the last decade, there is hope that the complexity of these processes will be better understood in the not-too-far future, providing an even better basis for simplified models such as the Babcock-Leighton approach. Still, we need to exercise caution and be aware of the severe limitations of all our efforts to understand the solar dynamo as lucidly expounded by Parker (2009) and Spruit (2011, 2012).

**Acknowledgments.** Sunspot data were obtained from the World Data Center SILSO, Royal Observatory of Belgium, Brussels. The data for the *aa*-index were obtained from [https://isgi.unistra.fr/indices\\_aa.php](https://isgi.unistra.fr/indices_aa.php)

## Ethics Declarations

### Competing interests

The authors declare they have no conflicts of interest.

## References

- Babcock HW (1961) The Topology of the Sun’s Magnetic Field and the 22-year Cycle. *Astrophys. J.* 133:572. <https://doi.org/10.1086/147060>
- Babcock HW, Babcock HD (1955) The Sun’s Magnetic Field, 1952-1954. *Astrophys. J.* 121:349. <https://doi.org/10.1086/145994>

- Barnes JA, Tryon PV, Sargent IH. H. (1980) Sunspot cycle simulation using random noise. In: Pepin RO, Eddy JA, Merrill RB (eds) *The Ancient Sun: Fossil Record in the Earth, Moon and Meteorites*, pp 159–163
- Basu S, Antia HM (2019) Changes in Solar Rotation over Two Solar Cycles. *Astrophys. J.* 883(1):93. <https://doi.org/10.3847/1538-4357/ab3b57>
- Baumann I, Schmitt D, Schüssler M, et al (2004) Evolution of the large-scale magnetic field on the solar surface: A parameter study. *Astron. Astrophys.* 426:1075–1091. <https://doi.org/10.1051/0004-6361:20048024>
- Bekki Y, Cameron RH (2022) Three-dimensional non-kinematic simulation of post-emergence evolution of bipolar magnetic regions and Babcock-Leighton dynamo of the Sun. arXiv e-prints arXiv:2209.08178. <https://doi.org/10.48550/arXiv.2209.08178>
- Bhowmik P, Nandy D (2018) Prediction of the strength and timing of sunspot cycle 25 reveal decadal-scale space environmental conditions. *Nature Communications* 9:5209. <https://doi.org/10.1038/s41467-018-07690-0>
- Bhowmik P, Jiang J, Upton L, et al (2023) Physical Models for Solar Cycle Predictions. *Space Sci. Rev.* p submitted. <https://doi.org/10.48550/arXiv.2303.12648>
- Bieber JW, Rust DM (1995) The Escape of Magnetic Flux from the Sun. *Astrophys. J.* 453:911. <https://doi.org/10.1086/176451>
- Birch AC, Schunker H, Braun DC, et al (2016) A low upper limit on the sub-surface rise speed of solar active regions. *Science Advances* 2(7):e1600,557–e1600,557. <https://doi.org/10.1126/sciadv.1600557>
- Biswas A, Karak BB, Cameron R (2022) Toroidal Flux Loss due to Flux Emergence Explains why Solar Cycles Rise Differently but Decay in a Similar Way. *Phys. Rev. Lett.* 129(24):241102. <https://doi.org/10.1103/PhysRevLett.129.241102>
- Biswas A, Karak B, Usoskin I, et al (2023) Long-term modulation of solar cycles. *Space Sci. Rev.* p in press. <https://doi.org/10.48550/arXiv.2302.14845>
- Brandenburg A (2005) The Case for a Distributed Solar Dynamo Shaped by Near-Surface Shear. *Astrophys. J.* 625(1):539–547. <https://doi.org/10.1086/429584>
- Brandenburg A, Elstner D, Masada Y, et al (2023) Turbulent processes and mean-field dynamo. arXiv e-prints arXiv:2303.12425. <https://doi.org/10.48550/arXiv.2303.12425>

- Brown TM, Christensen-Dalsgaard J, Dziembowski WA, et al (1989) Inferring the Sun's Internal Angular Velocity from Observed p-Mode Frequency Splittings. *Astrophys. J.* 343:526. <https://doi.org/10.1086/167727>
- Browning M, etal (2023) tbd. arXiv e-prints <https://doi.org/tbd>
- Brun AS, Browning MK (2017) Magnetism, dynamo action and the solar-stellar connection. *Liv. Rev. Sol. Phys.* 14:4. <https://doi.org/10.1007/s41116-017-0007-8>
- Caligari P, Moreno-Insertis F, Schüssler M (1995) Emerging Flux Tubes in the Solar Convection Zone. I. Asymmetry, Tilt, and Emergence Latitude. *Astrophys. J.* 441:886. <https://doi.org/10.1086/175410>
- Cameron R, Schüssler M (2015) The crucial role of surface magnetic fields for the solar dynamo. *Science* 347(6228):1333–1335. <https://doi.org/10.1126/science.1261470>
- Cameron RH, Schüssler M (2012) Are the strengths of solar cycles determined by converging flows towards the activity belts? *Astron. Astrophys.* 548:A57. <https://doi.org/10.1051/0004-6361/201219914>
- Cameron RH, Schüssler M (2016) The turbulent diffusion of toroidal magnetic flux as inferred from properties of the sunspot butterfly diagram. *Astron. Astrophys.* 591:A46. <https://doi.org/10.1051/0004-6361/201527284>
- Cameron RH, Schüssler M (2017a) An update of Leighton's solar dynamo model. *Astron. Astrophys.* 599:A52. <https://doi.org/https://doi.org/10.1051/0004-6361/201629746>
- Cameron RH, Schüssler M (2017b) Understanding Solar Cycle Variability. *Astrophys. J.* 843(2):111. <https://doi.org/10.3847/1538-4357/aa767a>
- Cameron RH, Schüssler M (2019) Solar activity: periodicities beyond 11 years are consistent with random forcing. *Astron. Astrophys.* 625:A28. <https://doi.org/https://doi.org/10.1051/0004-6361/201935290>
- Cameron RH, Schüssler M (2020) Loss of toroidal magnetic flux by emergence of bipolar magnetic regions. *Astron. Astrophys.* 636:A7. <https://doi.org/10.1051/0004-6361/201937281>
- Cameron RH, Schmitt D, Jiang J, et al (2012) Surface flux evolution constraints for flux transport dynamos. *Astron. Astrophys.* 542:A127. <https://doi.org/10.1051/0004-6361/201218906>
- Cameron RH, Dasi-Espuig M, Jiang J, et al (2013) Limits to solar cycle predictability: Cross-equatorial flux plumes. *Astron. Astrophys.* 557:A141.

<https://doi.org/https://doi.org/10.1051/0004-6361/201321981>

- Cameron RH, Jiang J, Schüssler M, et al (2014) Physical causes of solar cycle amplitude variability. *J. Geophys. Res.* 119(2):680–688. <https://doi.org/https://doi.org/10.1002/2013JA019498>
- Cameron RH, Jiang J, Schüssler M (2016) Solar Cycle 25: Another Moderate Cycle? *Astrophys. J. Lett.* 823(2):L22. <https://doi.org/10.3847/2041-8205/823/2/L22>
- Cameron RH, Duvall TL, Schüssler M, et al (2018) Observing and modeling the poloidal and toroidal fields of the solar dynamo. *Astron. Astrophys.* 609:A56. <https://doi.org/https://doi.org/10.1051/0004-6361/201731481>
- Cattaneo F, Vainshtein SI (1991) Suppression of Turbulent Transport by a Weak Magnetic Field. *Astrophys. J. Lett.* 376:L21. <https://doi.org/10.1086/186093>
- Centeno R (2012) The Naked Emergence of Solar Active Regions Observed with SDO/HMI. *Astrophys. J.* 759(1):72. <https://doi.org/10.1088/0004-637X/759/1/72>
- Charbonneau P (2020) Dynamo models of the solar cycle. *Liv. Rev. Sol. Phys.* 17(1):4. <https://doi.org/10.1007/s41116-020-00025-6>
- Charbonneau P, MacGregor KB (1997) Solar Interface Dynamos. II. Linear, Kinematic Models in Spherical Geometry. *Astrophys. J.* 486(1):502–520. <https://doi.org/10.1086/304485>
- Chatterjee P, Nandy D, Choudhuri AR (2004) Full-sphere simulations of a circulation-dominated solar dynamo: Exploring the parity issue. *Astron. Astrophys.* 427:1019–1030. <https://doi.org/10.1051/0004-6361:20041199>
- Chen F, Rempel M, Fan Y (2017) Emergence of Magnetic Flux Generated in a Solar Convective Dynamo. I. The Formation of Sunspots and Active Regions, and The Origin of Their Asymmetries. *Astrophys. J.* 846(2):149. <https://doi.org/10.3847/1538-4357/aa85a0>
- Choudhuri AR, Gilman PA (1987) The Influence of the Coriolis Force on Flux Tubes Rising through the Solar Convection Zone. *Astrophys. J.* 316:788. <https://doi.org/10.1086/165243>
- Choudhuri AR, Hazra G (2016) The treatment of magnetic buoyancy in flux transport dynamo models. *Advances in Space Research* 58(8):1560–1570. <https://doi.org/10.1016/j.asr.2016.03.015>
- Choudhuri AR, Schüssler M, Dikpati M (1995) The solar dynamo with



meridional circulation. *Astron. Astrophys.* 303:L29

- Christensen-Dalsgaard J, Monteiro MJPG, Rempel M, et al (2011) A more realistic representation of overshoot at the base of the solar convective envelope as seen by helioseismology. *Mon. Not. Roy. Astron. Soc.* 414(2):1158–1174. <https://doi.org/10.1111/j.1365-2966.2011.18460.x>
- Cowling TG (1953) *Solar Electrodynamics*. In: Kuiper GP (ed) *The Sun*. University of Chicago Press, p 532
- Dasi-Espuig M, Solanki SK, Krivova NA, et al (2010) Sunspot group tilt angles and the strength of the solar cycle. *Astron. Astrophys.* 518:A7. <https://doi.org/10.1051/0004-6361/201014301>
- David TJ, Angus R, Curtis JL, et al (2022) Further Evidence of Modified Spin-down in Sun-like Stars: Pileups in the Temperature-Period Distribution. *Astrophys. J.* 933(1):114. <https://doi.org/10.3847/1538-4357/ac6dd3>
- DeVore CR, Boris JP, Sheeley JN. R. (1984) The concentration of the large-scale solar magnetic field by a meridional surface flow. *Solar Phys.* 92(1-2):1–14. <https://doi.org/10.1007/BF00157230>
- Dikpati M, Charbonneau P (1999) A Babcock-Leighton Flux Transport Dynamo with Solar-like Differential Rotation. *Astrophys. J.* 518(1):508–520. <https://doi.org/10.1086/307269>
- Durney BR (1995) On a Babcock-Leighton dynamo model with a deep-seated generating layer for the toroidal magnetic field. *Solar Phys.* 160(2):213–235. <https://doi.org/10.1007/BF00732805>
- Durney BR (1997) On a Babcock-Leighton Solar Dynamo Model with a Deep-seated Generating Layer for the Toroidal Magnetic Field. IV. *Astrophys. J.* 486(2):1065–1077. <https://doi.org/10.1086/304546>
- Durrant CJ, Turner JPR, Wilson PR (2004) The Mechanism involved in the Reversals of the Sun’s Polar Magnetic Fields. *Solar Phys.* 222(2):345–362. <https://doi.org/10.1023/B:SOLA.0000043577.33961.82>
- Duvall JT. L. (1979) Large-scale solar velocity fields. *Solar Phys.* 63(1):3–15. <https://doi.org/10.1007/BF00155690>
- Fan Y (2021) Magnetic fields in the solar convection zone. *Liv. Rev. Sol. Phys.* 18(1):5. <https://doi.org/10.1007/s41116-021-00031-2>
- Fan Y, Fang F (2014) A Simulation of Convective Dynamo in the Solar Convective Envelope: Maintenance of the Solar-like Differential Rotation and Emerging Flux. *Astrophys. J.* 789(1):35. <https://doi.org/10.1088/>

0004-637X/789/1/35

- Fan Y, Fisher GH, McClymont AN (1994) Dynamics of Emerging Active Region Flux Loops. *Astrophys. J.* 436:907. <https://doi.org/10.1086/174967>
- Ferriz-Mas A, Schüssler M (1993) Instabilities of magnetic flux tubes in a stellar convection zone I. Equatorial flux rings in differentially rotating stars. *Geophysical and Astrophysical Fluid Dynamics* 72(1):209–247. <https://doi.org/10.1080/03091929308203613>
- Ferriz-Mas A, Schüssler M (1995) Instabilities of magnetic flux tubes in a stellar convection zone II. Flux rings outside the equatorial plane. *Geophysical and Astrophysical Fluid Dynamics* 81(3):233–265
- Gaizauskas V, Harvey KL, Harvey JW, et al (1983) Large-scale patterns formed by solar active regions during the ascending phase of cycle 21. *Astrophys. J.* 265:1056–1065. <https://doi.org/10.1086/160747>
- Galloway DJ, Weiss NO (1981) Convection and magnetic fields in stars. *Astrophys. J.* 243:945–953. <https://doi.org/10.1086/158659>
- Giovanelli RG (1985) The sunspot cycle and solar magnetic fields. I - The mechanism as inferred from observation. II - The interaction of flux tubes with the convection zone. *Australian Journal of Physics* 38:1045–1089. <https://doi.org/10.1071/PH851045>
- Gizon L, Duvall JT. L., Larsen RM (2001) Probing Surface Flows and Magnetic Activity with Time-Distance Helioseismology. In: Brekke P, Fleck B, Gurnman JB (eds) *Recent Insights into the Physics of the Sun and Heliosphere: Highlights from SOHO and Other Space Missions*, p 189
- Gizon L, Cameron R, Pourabedian M, et al (2020) Meridional flow in the Sun’s convection zone is a single cell in each hemisphere. *Science* 368(6498):1469–1472. <https://doi.org/https://doi.org/10.1126/science.aaz7119>
- Gottschling N, Schunker H, Birch AC, et al (2021) Evolution of solar surface inflows around emerging active regions. *Astron. Astrophys.* 652:A148. <https://doi.org/10.1051/0004-6361/202140324>
- Guckenheimer J, Holmes P (1983) *Nonlinear oscillations, dynamical systems, and bifurcations of vector fields.* Applied mathematical sciences, Springer, New York
- Guerrero G, de Gouveia Dal Pino EM (2007) How does the shape and thickness of the tachocline affect the distribution of the toroidal magnetic fields in the solar dynamo? *Astron. Astrophys.* 464(1):341–349. <https://doi.org/10.1051/0004-6361:20065834>

- Guerrero G, Dikpati M, de Gouveia Dal Pino EM (2009) The Role of Diffusivity Quenching in Flux-transport Dynamo Models. *Astrophys. J.* 701(1):725–736. <https://doi.org/10.1088/0004-637X/701/1/725>
- Hale GE, Ellerman F, Nicholson SB, et al (1919) The Magnetic Polarity of Sun-Spots. *Astrophys. J.* 49:153. <https://doi.org/10.1086/142452>
- Hanasoge SM (2022) Surface and interior meridional circulation in the Sun. *Liv. Rev. Sol. Phys.* 19(1):3. <https://doi.org/10.1007/s41116-022-00034-7>
- Harvey KL (1993) Magnetic bipoles on the Sun. PhD thesis, University of Utrecht, Netherlands
- Harvey KL, Harvey JW, Martin SF (1975) Ephemeral Active Regions in 1970 and 1973. *Solar Phys.* 40(1):87–102. <https://doi.org/10.1007/BF00183154>
- Hathaway DH (2011) A Standard Law for the Equatorward Drift of the Sunspot Zones. *Solar Phys.* 273(1):221–230. <https://doi.org/10.1007/s11207-011-9837-z>
- Hathaway DH (2015) The Solar Cycle. *Liv. Rev. Sol. Phys.* 12(1):4. <https://doi.org/10.1007/lrsp-2015-4>
- Hathaway DH, Upton LA (2016) Predicting the amplitude and hemispheric asymmetry of solar cycle 25 with surface flux transport. *Journal of Geophysical Research (Space Physics)* 121(11):10,744–10,753. <https://doi.org/10.1002/2016JA023190>
- Hathaway DH, Upton LA, Mahajan SS (2022) Variations in differential rotation and meridional flow within the Sun’s surface shear layer 1996–2022. *Frontiers in Astronomy and Space Sciences* 9:419. <https://doi.org/10.3389/fspas.2022.1007290>
- Hazra G (2021) Recent advances in the 3D kinematic Babcock-Leighton solar dynamo modeling. *Journal of Astrophysics and Astronomy* 42(2):22. <https://doi.org/10.1007/s12036-021-09738-y>
- Hazra G, Miesch MS (2018) Incorporating Surface Convection into a 3D Babcock-Leighton Solar Dynamo Model. *Astrophys. J.* 864(2):110. <https://doi.org/10.3847/1538-4357/aad556>
- Hazra G, Choudhuri AR, Miesch MS (2017) A Theoretical Study of the Build-up of the Sun’s Polar Magnetic Field by using a 3D Kinematic Dynamo Model. *Astrophys. J.* 835(1):39. <https://doi.org/10.3847/1538-4357/835/1/39>

- Hazra G, Nandy D, Kitchatinov L, et al (2023) Mean field models of flux transport dynamo and meridional circulation in the Sun and stars. *Space Sci. Rev.* p submitted. <https://doi.org/10.48550/arXiv.2302.09390>
- Hotta H (2017) Solar Overshoot Region and Small-scale Dynamo with Realistic Energy Flux. *Astrophys. J.* 843(1):52. <https://doi.org/10.3847/1538-4357/aa784b>
- Howard R (1979) Evidence for large-scale velocity features on the sun. *Astrophys. J. Lett.* 228:L45–L50. <https://doi.org/10.1086/182900>
- Howard RF (1996) Solar Active Regions As Diagnostics of Subsurface Conditions. *Ann. Rev. Astron. Astrophys.* 34:75–110. <https://doi.org/10.1146/annurev.astro.34.1.75>
- Howe R (2009) Solar Interior Rotation and its Variation. *Liv. Rev. Sol. Phys.* 6(1):1. <https://doi.org/10.12942/lrsp-2009-1>
- Hubbard A, Brandenburg A (2012) Catastrophic Quenching in  $\alpha\Omega$  Dynamos Revisited. *Astrophys. J.* 748(1):51. <https://doi.org/10.1088/0004-637X/748/1/51>
- Isik E, etal (2023) tbd. arXiv e-prints <https://doi.org/tbd>
- Jefferers SV, Cameron RH, Marsden SC, et al (2022) The crucial role of surface magnetic fields for stellar dynamos:  $\epsilon$  Eridani, 61 Cygni A, and the Sun. *Astron. Astrophys.* 661:A152. <https://doi.org/https://doi.org/10.1051/0004-6361/202142202>
- Jiang J (2020) Nonlinear Mechanisms that Regulate the Solar Cycle Amplitude. *Astrophys. J.* 900(1):19. <https://doi.org/10.3847/1538-4357/abaa4b>
- Jiang J, Cameron RH, Schüssler M (2014a) Effects of the Scatter in Sunspot Group Tilt Angles on the Large-scale Magnetic Field at the Solar Surface. *Astrophys. J.* 791(1):5. <https://doi.org/10.1088/0004-637X/791/1/5>
- Jiang J, Hathaway DH, Cameron RH, et al (2014b) Magnetic Flux Transport at the Solar Surface. *Space Sci. Rev.* 186(1-4):491–523. <https://doi.org/10.1007/s11214-014-0083-1>
- Jiang J, Cameron RH, Schüssler M (2015) The Cause of the Weak Solar Cycle 24. *Astrophys. J. Lett.* 808(1):L28. <https://doi.org/https://doi.org/10.1088/2041-8205/808/1/L28>
- Jiang J, Wang JX, Jiao QR, et al (2018) Predictability of the Solar Cycle Over One Cycle. *Astrophys. J.* 863(2):159. <https://doi.org/10.3847/1538-4357/aad197>

- Jiao Q, Jiang J, Wang ZF (2021) Sunspot tilt angles revisited: Dependence on the solar cycle strength. *Astron. Astrophys.* 653:A27. <https://doi.org/10.1051/0004-6361/202141215>
- Karak B (2023) Models for the long-term variations of solar activity. *Liv. Rev. Sol. Phys.* p in press
- Karak BB, Cameron R (2016) Babcock-Leighton Solar Dynamo: The Role of Downward Pumping and the Equatorward Propagation of Activity. *Astrophys. J.* 832(1):94. <https://doi.org/10.3847/0004-637X/832/1/94>
- Karak BB, Miesch M (2017) Solar Cycle Variability Induced by Tilt Angle Scatter in a Babcock-Leighton Solar Dynamo Model. *Astrophys. J.* 847(1):69. <https://doi.org/10.3847/1538-4357/aa8636>
- Kitchatinov L, Nepomnyashchikh A (2017) How supercritical are stellar dynamos, or why do old main-sequence dwarfs not obey gyrochronology? *Mon. Not. Roy. Astron. Soc.* 470(3):3124–3130. <https://doi.org/10.1093/mnras/stx1473>
- Kitchatinov LL, Olemskoy SV (2011a) Alleviation of catastrophic quenching in solar dynamo model with nonlocal alpha-effect. *Astron. Nachr.* 332(5):496. <https://doi.org/10.1002/asna.201011549>
- Kitchatinov LL, Olemskoy SV (2011b) Does the Babcock-Leighton mechanism operate on the Sun? *Astronomy Letters* 37(9):656–658. <https://doi.org/10.1134/S0320010811080031>
- Kitchatinov LL, Mordvinov AV, Nepomnyashchikh AA (2018) Modelling variability of solar activity cycles. *Astron. Astrophys.* 615:A38. <https://doi.org/10.1051/0004-6361/201732549>
- Kleeorin N, Rogachevskii I (2007) Nonlinear turbulent magnetic diffusion and effective drift velocity of a large-scale magnetic field in two-dimensional magnetohydrodynamic turbulence. *Phys. Rev. E* 75(6):066315. <https://doi.org/10.1103/PhysRevE.75.066315>
- Kleeorin N, Moss D, Rogachevskii I, et al (2000) Helicity balance and steady-state strength of the dynamo generated galactic magnetic field. *Astron. Astrophys.* 361:L5–L8. <https://doi.org/10.48550/arXiv.astro-ph/0205266>
- Köhler H (1973) The Solar Dynamo and Estimate of the Magnetic Diffusivity and the  $\alpha$ -effect. *Astron. Astrophys.* 25:467
- Kotorashvili K, Blackman EG, Owen JE (2023) Why the observed spin evolution of older-than-solar like stars might not require a dynamo mode change. *arXiv e-prints arXiv:2301.04693*. <https://arxiv.org/abs/2301.04693>

[astro-ph.SR]

- Kumar P, Nagy M, Lemerle A, et al (2021) The Polar Precursor Method for Solar Cycle Prediction: Comparison of Predictors and Their Temporal Range. *Astrophys. J.* 909(1):87. <https://doi.org/10.3847/1538-4357/abdbb4>
- Kumar R, Jouve L, Nandy D (2019) A 3D kinematic Babcock Leighton solar dynamo model sustained by dynamic magnetic buoyancy and flux transport processes. *Astron. Astrophys.* 623:A54. <https://doi.org/10.1051/0004-6361/201834705>
- Labonte BJ, Howard R (1982) Torsional Waves on the Sun and the Activity Cycle. *Solar Phys.* 75(1-2):161–178. <https://doi.org/10.1007/BF00153469>
- Larson TP, Schou J (2018) Global-Mode Analysis of Full-Disk Data from the Michelson Doppler Imager and the Helioseismic and Magnetic Imager. *Solar Phys.* 293(2):29. <https://doi.org/10.1007/s11207-017-1201-5>
- Legrand JP, Simon PA (1981) Ten Cycles of Solar and Geomagnetic Activity. *Solar Phys.* 70(1):173–195. <https://doi.org/https://doi.org/10.1007/BF00154399>
- Leighton RB (1964) Transport of Magnetic Fields on the Sun. *Astrophys. J.* 140:1547. <https://doi.org/10.1086/148058>
- Leighton RB (1969) A Magneto-Kinematic Model of the Solar Cycle. *Astrophys. J.* 156:1. <https://doi.org/https://doi.org/10.1086/149943>
- Lemerle A, Charbonneau P (2017) A Coupled  $2 \times 2$ D Babcock-Leighton Solar Dynamo Model. II. Reference Dynamo Solutions. *Astrophys. J.* 834(2):133. <https://doi.org/10.3847/1538-4357/834/2/133>
- Lemerle A, Charbonneau P, Carignan-Dugas A (2015) A Coupled  $2 \times 2$ D Babcock-Leighton Solar Dynamo Model. I. Surface Magnetic Flux Evolution. *Astrophys. J.* 810(1):78. <https://doi.org/10.1088/0004-637X/810/1/78>
- Liu AL, Scherrer PH (2022) Solar Toroidal Field Evolution Spanning Four Sunspot Cycles Seen by the Wilcox Solar Observatory, the Solar and Heliospheric Observatory/Michelson Doppler Imager, and the Solar Dynamics Observatory/Helioseismic and Magnetic Imager. *Astrophys. J. Lett.* 927(1):L2. <https://doi.org/10.3847/2041-8213/ac52ae>
- Longcope DW, Fisher GH (1996) The Effects of Convection Zone Turbulence on the Tilt Angles of Magnetic Bipoles. *Astrophys. J.* 458:380. <https://doi.org/10.1086/176821>

- Mackay DH, Yeates AR (2012) The Sun's Global Photospheric and Coronal Magnetic Fields: Observations and Models. *Liv. Rev. Sol. Phys.* 9(1):6. <https://doi.org/10.12942/lrsp-2012-6>
- Mandal S, Karak B, Banerjee D (2017) Latitude Distribution of Sunspots: Analysis Using Sunspot Data and a Dynamo Model. *Astrophys. J.* 851(1):70. <https://doi.org/10.3847/1538-4357/aa97dc>
- Martin SF, Harvey KH (1979) Ephemeral Active Regions during Solar Minimum. *Solar Phys.* 64(1):93–108. <https://doi.org/10.1007/BF00151118>
- Martin-Belda D, Cameron RH (2016) Surface flux transport simulations: Effect of inflows toward active regions and random velocities on the evolution of the Sun's large-scale magnetic field. *Astron. Astrophys.* 586:A73. <https://doi.org/10.1051/0004-6361/201527213>
- Martin-Belda D, Cameron RH (2017) Inflows towards active regions and the modulation of the solar cycle: A parameter study. *Astron. Astrophys.* 597:A21. <https://doi.org/10.1051/0004-6361/201629061>
- McClintock BH, Norton AA (2013) Recovering Joy's Law as a Function of Solar Cycle, Hemisphere, and Longitude. *Solar Phys.* 287(1-2):215–227. <https://doi.org/10.1007/s11207-013-0338-0>
- McClintock BH, Norton AA (2016) Tilt Angle and Footpoint Separation of Small and Large Bipolar Sunspot Regions Observed with HMI. *Astrophys. J.* 818(1):7. <https://doi.org/10.3847/0004-637X/818/1/7>
- Metcalfe TS, Egeland R, van Saders J (2016) Stellar Evidence That the Solar Dynamo May Be in Transition. *Astrophys. J. Lett.* 826(1):L2. <https://doi.org/10.3847/2041-8205/826/1/L2>
- Metcalfe TS, Finley AJ, Kochukhov O, et al (2022) The Origin of Weakened Magnetic Braking in Old Solar Analogs. *Astrophys. J. Lett.* 933(1):L17. <https://doi.org/10.3847/2041-8213/ac794d>
- Metcalfe TS, Strassmeier KG, Ilyin IV, et al (2023) Constraints on Magnetic Braking from the G8 Dwarf Stars 61 UMa and  $\tau$  Cet. *arXiv e-prints arXiv:2304.09896*. <https://doi.org/10.48550/arXiv.2304.09896>
- Miesch MS, Dikpati M (2014) A Three-dimensional Babcock-Leighton Solar Dynamo Model. *Astrophys. J. Lett.* 785(1):L8. <https://doi.org/10.1088/2041-8205/785/1/L8>
- Moreno-Insertis F, Schüssler M, Ferriz-Mas A (1992) Storage of magnetic flux tubes in a convective overshoot region. *Astron. Astrophys.* 264(2):686–700

- Muñoz-Jaramillo A, Nandy D, Martens PCH (2009) Helioseismic Data Inclusion in Solar Dynamo Models. *Astrophys. J.* 698(1):461–478. <https://doi.org/10.1088/0004-637X/698/1/461>
- Muñoz-Jaramillo A, Nandy D, Martens PCH, et al (2010) A Doubling Algorithm for Modeling Solar Active Regions: Unifying Kinematic Dynamo Models and Surface Flux-transport Simulations. *Astrophys. J. Lett.* 720(1):L20–L25. <https://doi.org/10.1088/2041-8205/720/1/L20>
- Muñoz-Jaramillo A, Dasi-Espuig M, Balmaceda LA, et al (2013) Solar Cycle Propagation, Memory, and Prediction: Insights from a Century of Magnetic Proxies. *Astrophys. J. Lett.* 767(2):L25. <https://doi.org/10.1088/2041-8205/767/2/L25>
- Nagy M, Lemerle A, Labonville F, et al (2017) The Effect of “Rogue” Active Regions on the Solar Cycle. *Solar Phys.* 292(11):167. <https://doi.org/10.1007/s11207-017-1194-0>
- Nagy M, Lemerle A, Charbonneau P (2020) Impact of nonlinear surface inflows into activity belts on the solar dynamo. *Journal of Space Weather and Space Climate* 10:62. <https://doi.org/10.1051/swsc/2020064>
- Nandy D, Choudhuri AR (2001) Toward a Mean Field Formulation of the Babcock-Leighton Type Solar Dynamo. I.  $\alpha$ -Coefficient versus Durney’s Double-Ring Approach. *Astrophys. J.* 551(1):576–585. <https://doi.org/10.1086/320057>
- Nandy D, Choudhuri AR (2002) Explaining the Latitudinal Distribution of Sunspots with Deep Meridional Flow. *Science* 296(5573):1671–1673. <https://doi.org/10.1126/science.1070955>
- Nelson NJ, Brown BP, Sacha Brun A, et al (2014) Buoyant Magnetic Loops Generated by Global Convective Dynamo Action. *Solar Phys.* 289(2):441–458. <https://doi.org/10.1007/s11207-012-0221-4>
- Parker EN (1955a) Hydromagnetic Dynamo Models. *Astrophys. J.* 122:293. <https://doi.org/10.1086/146087>
- Parker EN (1955b) The Formation of Sunspots from the Solar Toroidal Field. *Astrophys. J.* 121:491. <https://doi.org/10.1086/146010>
- Parker EN (1975) The generation of magnetic fields in astrophysical bodies. X. Magnetic buoyancy and the solar dynamo. *Astrophys. J.* 198:205–209. <https://doi.org/10.1086/153593>
- Parker EN (1984) Magnetic buoyancy and the escape of magnetic fields from stars. *Astrophys. J.* 281:839–845. <https://doi.org/10.1086/162163>



- Parker EN (1993) A Solar Dynamo Surface Wave at the Interface between Convection and Nonuniform Rotation. *Astrophys. J.* 408:707. <https://doi.org/10.1086/172631>
- Parker EN (2009) Solar Magnetism: The State of Our Knowledge and Ignorance. *Space Sci. Rev.* 144(1-4):15–24. <https://doi.org/10.1007/s11214-008-9445-x>
- Petrovay K (2020) Solar cycle prediction. *Liv. Rev. Sol. Phys.* 17(1):2. <https://doi.org/10.1007/s41116-020-0022-z>
- Petrovay K, Nagy M, Yeates AR (2020) Towards an algebraic method of solar cycle prediction. I. Calculating the ultimate dipole contributions of individual active regions. *Journal of Space Weather and Space Climate* 10:50. <https://doi.org/10.1051/swsc/2020050>
- Pipin VV (2022) On the effect of surface bipolar magnetic regions on the convection zone dynamo. *Mon. Not. Roy. Astron. Soc.* 514(1):1522–1534. <https://doi.org/10.1093/mnras/stac1434>
- Reiners A, Shulyak D, Käpylä PJ, et al (2022) Magnetism, rotation, and non-thermal emission in cool stars. Average magnetic field measurements in 292 M dwarfs. *Astron. Astrophys.* 662:A41. <https://doi.org/10.1051/0004-6361/202243251>
- Rempel M (2006) Flux-Transport Dynamos with Lorentz Force Feedback on Differential Rotation and Meridional Flow: Saturation Mechanism and Torsional Oscillations. *Astrophys. J.* 647(1):662–675. <https://doi.org/10.1086/505170>
- Route M (2016) The Discovery of Solar-like Activity Cycles Beyond the End of the Main Sequence? *Astrophys. J. Lett.* 830(2):L27. <https://doi.org/10.3847/2041-8205/830/2/L27>
- Rüdiger G, Brandenburg A (1995) A solar dynamo in the overshoot layer: cycle period and butterfly diagram. *Astron. Astrophys.* 296:557
- Schatten KH, Scherrer PH, Svalgaard L, et al (1978) Using Dynamo Theory to predict the sunspot number during Solar Cycle 21. *Geophys. Res. Lett.* 5(5):411–414. <https://doi.org/10.1029/GL005i005p00411>
- Schunker H, Braun DC, Birch AC, et al (2016) SDO/HMI survey of emerging active regions for helioseismology. *Astron. Astrophys.* 595:A107. <https://doi.org/10.1051/0004-6361/201628388>
- Schunker H, Birch AC, Cameron RH, et al (2019) Average motion of emerging solar active region polarities. I. Two phases of emergence. *Astron. Astrophys.*

625:A53. <https://doi.org/10.1051/0004-6361/201834627>

Schunker H, Baumgartner C, Birch AC, et al (2020) Average motion of emerging solar active region polarities. II. Joy's law. *Astron. Astrophys.* 640:A116. <https://doi.org/10.1051/0004-6361/201937322>

Schüssler M, Rempel M (2005) The dynamical disconnection of sunspots from their magnetic roots. *Astron. Astrophys.* 441(1):337–346. <https://doi.org/10.1051/0004-6361:20052962>

Schüssler M, Caligari P, Ferriz-Mas A, et al (1994) Instability and eruption of magnetic flux tubes in the solar convection zone. *Astron. Astrophys.* 281:L69–L72

Solanki SK, Usoskin IG, Kromer B, et al (2004) Unusual activity of the Sun during recent decades compared to the previous 11,000 years. *Nature* 431(7012):1084–1087. <https://doi.org/10.1038/nature02995>

Solanki SK, Wenzler T, Schmitt D (2008) Moments of the latitudinal dependence of the sunspot cycle: a new diagnostic of dynamo models. *Astron. Astrophys.* 483(2):623–632. <https://doi.org/10.1051/0004-6361:20054282>

Spruit HC (1997) Convection in stellar envelopes: a changing paradigm. *Memorie della Societa Astronomica Italiana* 68:397–413. <https://doi.org/10.48550/arXiv.astro-ph/9605020>

Spruit HC (2011) Theories of the Solar Cycle: A Critical View. In: Miralles MP, Sánchez Almeida J (eds) *The Sun, the Solar Wind, and the Heliosphere*, vol 4. Springer, Dordrecht, p 39

Spruit HC (2012) Theories of the Solar Cycle and Its Effect on Climate. *Progress of Theoretical Physics Supplement* 195:185–200. <https://doi.org/10.1143/PTPS.195.185>

Spruit HC, van Ballegoijen AA (1982) Stability of toroidal flux tubes in stars. *Astron. Astrophys.* 106(1):58–66

Steenbeck M, Krause F (1966) Erklärung stellarer und planetarer Magnetfelder durch einen turbulenzbedingten Dynamomechanismus. *Zs Naturforsch A* 21:1285. <https://doi.org/10.1515/zna-1966-0813>

Steenbeck M, Krause F (1969) On the Dynamo Theory of Stellar and Planetary Magnetic Fields. I. AC Dynamos of Solar Type. *Astron. Nachr.* 291:49–84. <https://doi.org/10.1002/asna.19692910201>

- Steenbeck M, Krause F, Rädler KH (1966) Berechnung der mittleren Lorentz-Feldstärke für ein elektrisch leitendes Medium in turbulenter, durch Coriolis-Kräfte beeinflusster Bewegung. *Zeitschrift Naturforschung Teil A* 21:369. <https://doi.org/10.1515/zna-1966-0401>
- Stix M (1972) Non-Linear Dynamo Waves. *Astron. Astrophys.* 20:9
- Talafha M, Nagy M, Lemerle A, et al (2022) Role of observable nonlinearities in solar cycle modulation. *Astron. Astrophys.* 660:A92. <https://doi.org/10.1051/0004-6361/202142572>
- Tobias SM (1996) Diffusivity Quenching as a Mechanism for Parker's Surface Dynamo. *Astrophys. J.* 467:870. <https://doi.org/10.1086/177661>
- Tobias SM, Weiss NO, Kirk V (1995) Chaotically modulated stellar dynamos. *Mon. Not. Roy. Astron. Soc.* 273(4):1150–1166. <https://doi.org/10.1093/mnras/273.4.1150>
- Tripathi B, Nandy D, Banerjee S (2021) Stellar mid-life crisis: subcritical magnetic dynamos of solar-like stars and the breakdown of gyrochronology. *Mon. Not. Roy. Astron. Soc.* 506(1):L50–L54. <https://doi.org/10.1093/mnrasl/slab035>
- Upton L, Hathaway DH (2014) Predicting the Sun's Polar Magnetic Fields with a Surface Flux Transport Model. *Astrophys. J.* 780(1):5. <https://doi.org/10.1088/0004-637X/780/1/5>
- Usoskin IG (2017) A history of solar activity over millennia. *Liv. Rev. Sol. Phys.* 14(1):3. <https://doi.org/10.1007/s41116-017-0006-9>
- Usoskin IG, Gallet Y, Lopes F, et al (2016) Solar activity during the Holocene: the Hallstatt cycle and its consequence for grand minima and maxima. *Astron. Astrophys.* 587:A150. <https://doi.org/10.1051/0004-6361/201527295>
- van Saders JL, Ceillier T, Metcalfe TS, et al (2016) Weakened magnetic braking as the origin of anomalously rapid rotation in old field stars. *Nature* 529(7585):181. <https://doi.org/10.1038/nature16168>
- Waldmeier M (1939) Die Zonenwanderung der Sonnenflecken. *Astron. Mitt. Eidgen. Sternw. Zürich* 14:470–481
- Waldmeier M (1955) *Ergebnisse und Probleme der Sonnenforschung.*
- Wallenhorst SG, Topka KP (1982) On the Disappearance of a Small Sunspot Group. *Solar Phys.* 81(1):33–46. <https://doi.org/10.1007/BF00151977>

- Wang YM, Sheeley JN. R. (1991) Magnetic Flux Transport and the Sun's Dipole Moment: New Twists to the Babcock-Leighton Model. *Astrophys. J.* 375:761. <https://doi.org/10.1086/170240>
- Wang YM, Sheeley NR (2009) Understanding the Geomagnetic Precursor of the Solar Cycle. *Astrophys. J. Lett.* 694(1):L11–L15. <https://doi.org/10.1088/0004-637X/694/1/L11>
- Wang YM, Nash AG, Sheeley JN. R. (1989a) Evolution of the Sun's Polar Fields during Sunspot Cycle 21: Poleward Surges and Long-Term Behavior. *Astrophys. J.* 347:529. <https://doi.org/10.1086/168143>
- Wang YM, Nash AG, Sheeley JN. R. (1989b) Magnetic Flux Transport on the Sun. *Science* 245(4919):712–718. <https://doi.org/10.1126/science.245.4919.712>
- Wang YM, Sheeley JN. R., Nash AG (1991) A New Solar Cycle Model Including Meridional Circulation. *Astrophys. J.* 383:431. <https://doi.org/10.1086/170800>
- Wang YM, Sheeley JN. R., Lean J (2002) Meridional Flow and the Solar Cycle Variation of the Sun's Open Magnetic Flux. *Astrophys. J.* 580(2):1188–1196. <https://doi.org/10.1086/343845>
- Whitbread T, Yeates AR, Muñoz-Jaramillo A, et al (2017) Parameter optimization for surface flux transport models. *Astron. Astrophys.* 607:A76. <https://doi.org/10.1051/0004-6361/201730689>
- Whitbread T, Yeates AR, Muñoz-Jaramillo A (2018) How Many Active Regions Are Necessary to Predict the Solar Dipole Moment? *Astrophys. J.* 863(2):116. <https://doi.org/10.3847/1538-4357/aad17e>
- Whitbread T, Yeates AR, Muñoz-Jaramillo A (2019) The need for active region disconnection in 3D kinematic dynamo simulations. *Astron. Astrophys.* 627:A168. <https://doi.org/10.1051/0004-6361/201935986>
- Wilson PR, Altrocki RC, Harvey KL, et al (1988) The extended solar activity cycle. *Nature* 333(6175):748–750. <https://doi.org/10.1038/333748a0>
- Wright NJ, Drake JJ (2016) Solar-type dynamo behaviour in fully convective stars without a tachocline. *Nature* 535(7613):526–528. <https://doi.org/10.1038/nature18638>
- Yeates AR, Muñoz-Jaramillo A (2013) Kinematic active region formation in a three-dimensional solar dynamo model. *Mon. Not. Roy. Astron. Soc.* 436(4):3366–3379. <https://doi.org/10.1093/mnras/stt1818>

- Yeates AR, Nandy D, Mackay DH (2008) Exploring the Physical Basis of Solar Cycle Predictions: Flux Transport Dynamics and Persistence of Memory in Advection- versus Diffusion-dominated Solar Convection Zones. *Astrophys. J.* 673(1):544–556. <https://doi.org/10.1086/524352>
- Yeates AR, Cheung MCM, Jiang J, et al (2023) Surface Flux Transport. *Space Sci. Rev.* p submitted. <https://doi.org/10.48550/arXiv.2303.01209>
- Yoshimura H (1975) Solar-cycle dynamo wave propagation. *Astrophys. J.* 201:740–748. <https://doi.org/10.1086/153940>
- Yule GU (1927) On a Method of Investigating Periodicities in Disturbed Series, with special reference to Wolfer's Sunspot Numbers. *Phil Trans Roy Soc London A* 226:267–298
- Zhang Z, Jiang J (2022) A Babcock-Leighton-type Solar Dynamo Operating in the Bulk of the Convection Zone. *Astrophys. J.* 930(1):30. <https://doi.org/10.3847/1538-4357/ac6177>